On rapid oscillations driving biological processes at disparate timescales

Davin Lunz

On rapid oscillations driving biological processes at disparate timescales

D. Lunz

E-mail: davin.lunz@polytechnique.edu
INRIA Saclay – Île de France, 91120 Palaiseau, France
École Polytechnique, CMAP 91128 Palaiseau, France
Institut Pasteur, 75015 Paris, France

Abstract. We consider a generic biological process described by a dynamical system, subject to an input signal with a high-frequency periodic component. The rapid oscillations of the input signal induce inherently multiscale dynamics, motivating order-reduction techniques. It is intuitive that the system behaviour is well approximated by its response to the averaged input signal. However, changes to the high-frequency component that preserve the average signal are beyond the reach of such intuitive reasoning. In this study, we explore system response under the influence of such an input signal by exploiting the timescale separation between high-frequency input variations and system response time. Employing the asymptotic method of multiple scales, we establish that, in some circumstances, the intuitive approach is simply the leading-order asymptotic contribution. We focus on higher-order corrections that capture the response to the details of the high-frequency component beyond its average. This approach achieves a reduction in system complexity while providing valuable insight into the structure of the response to the oscillations. We develop the general theory for nonlinear systems, while highlighting the important case of systems affine in the state and the input signal, presenting examples of both discrete and continuum state spaces. Importantly, this class of systems encompasses biochemical reaction networks described by the chemical master equation and its continuum approximations. Finally, we apply the framework to a nonlinear system describing mRNA translation and protein expression previously studied in the literature. The analysis shines new light on several aspects of the system quantification and both extends and simplifies results previously obtained.

1. Introduction

Timescale separation — where different system processes unfold over vastly different timescales — is a common phenomenon across the biological, chemical, and physical sciences [1, 2]. The challenge in accurately modeling systems exhibiting timescale separation is that they are inherently multiscale, requiring fine-grained resolution of phenomena occurring over fast timescales to be carried out over long time horizons on which the slow phenomena evolve. This makes systems with timescale separation prime candidates for model reduction and approximation methods. The general form for such a system can be written as

$$\frac{\mathrm{d}\boldsymbol{y}}{\mathrm{d}t} = \boldsymbol{f}(\boldsymbol{y},\boldsymbol{x},t), \qquad \boldsymbol{y}(0) = \boldsymbol{y}^0, \tag{1a}$$

$$\varepsilon\frac{\mathrm{d}\boldsymbol{x}}{\mathrm{d}t} = \boldsymbol{g}(\boldsymbol{y},\boldsymbol{x},t), \qquad \boldsymbol{x}(0) = \boldsymbol{x}^0. \tag{1b}$$

where $\varepsilon \ll 1$ is a small parameter, $\boldsymbol{y}(t)$ and $\boldsymbol{x}(t)$ are vector-valued functions of time, with initial conditions $\boldsymbol{y}^0$ and $\boldsymbol{x}^0$, respectively, and $\boldsymbol{f}$ and $\boldsymbol{g}$ are general operators describing the system dynamics. If non-dimensionalised appropriately, such that the terms on the right-hand side of (1) are of order unity, then the factor of ε multiplying the $\mathrm{d}\boldsymbol{x}/\mathrm{d}t$ term suggests that the variation in $\boldsymbol{x}$ per unit time is typically large. This is interpreted to mean that the dynamics associated with $\boldsymbol{x}$ are fast, and hence we call $\boldsymbol{x}$ the fast species and $\boldsymbol{y}$ the slow species.

One particularly well studied approximation technique is the quasi-steady-state assumption [3] (QSSA), that forms the basis for Michaelis–Menten enzyme kinetics [4], and is used extensively in general chemical kinetic simulation [5, 6, 7, 8] and analysis [9, 10, 11, 12, 13, 14, 15]. The idea is based on the aforementioned quantitative observation: the fast species $\boldsymbol{x}$ will equilibrate to their stationary distributions over a rapid timescale, during which the slow species $\boldsymbol{y}$ remain essentially constant. Thus, on the slow timescale, the fast species may be approximated by their quasi-steady-state by setting the left-hand side of (1b) to zero to obtain the governing algebraic relation $\boldsymbol{g}(\boldsymbol{y},\boldsymbol{x},t) = 0$. This reduces the model to purely slow dynamics without needing to resolve the fast timescale. Other than perhaps a boundary layer in early time, this assumption provides an accurate approximation scheme [3].

While the underlying intuition — that fast reactions may be approximated by their quasi-steady state — is convincing, it remains hazy how to systematically improve the approximation accuracy or estimate its inaccuracy. The key is to recognise that, mathematically, the QSSA is an application of singular perturbation theory [16, 17, 18]. The system dynamics are approximated asymptotically in the limit as the timescale separation (that is, the ratio between the slow and fast timescales, $1/\varepsilon$) tends to infinity. The QSSA is nothing other than the leading-order term of the asymptotic expansion. Within this general framework, contributions of arbitrarily high order may be systematically determined alongside formal error approximations [19]. As is well known [3], a consequence of approximating the fast variables by their quasi-steady state is that they cannot satisfy arbitrary initial conditions. It is for this reason that the asymptotics are called singular. There is a boundary layer in time, that is, a transient interval over which the initial condition converges toward its quasi-steady state. The theory of matched asymptotic expansions allows these boundary layers to be resolved systematically to arbitrarily high order [16].

In this study, we are concerned with a phenomenon that is related to, but different from, the classical fast–slow systems. Motivated by the prevalence in biological systems of synthetic [20] or natural [21] oscillatory signals, we focus on systems with an input signal, or a system parameter, that varies periodically on a timescale significantly faster than the timescale of interest. Including this in the classical system (1), the system dynamics may be

written as

$$\frac{\mathrm{d}\boldsymbol{y}}{\mathrm{d}t} = \boldsymbol{f}(\boldsymbol{y},\boldsymbol{x},\boldsymbol{u}(t/\varepsilon),t), \qquad \boldsymbol{y}(0) = \boldsymbol{y}^0, \tag{2a}$$

$$\varepsilon\frac{\mathrm{d}\boldsymbol{x}}{\mathrm{d}t} = \boldsymbol{g}(\boldsymbol{y},\boldsymbol{x},\boldsymbol{u}(t/\varepsilon),t), \qquad \boldsymbol{x}(0) = \boldsymbol{x}^0, \tag{2b}$$

for some known vector-valued function $\boldsymbol{u}$ that is of order unity and varying on a timescale of order unity. For concreteness, it may be helpful to think of the scalar-valued $u(\tau) = \sin(\tau)$, however, our analysis deals with the general case. For trivial $\boldsymbol{u}$, problem (2) reduces to (1), and thus (2) is no less general than (1). It might be tempting to think that the converse also holds, whereby we may cast the problem (2) in the framework of (1) by augmenting the fast state variable $\boldsymbol{x}$ via $\hat{\boldsymbol{x}}(t) = (\boldsymbol{x}(t),\boldsymbol{u}(t/\varepsilon))$ whose time derivative (multiplied by ε) is given by $\hat{\boldsymbol{g}}(\boldsymbol{y},\hat{\boldsymbol{x}},t) := (\boldsymbol{g}(\boldsymbol{y},\boldsymbol{x},\boldsymbol{u}(t/\varepsilon),t),\boldsymbol{u}'(t/\varepsilon))$ with initial condition $\hat{\boldsymbol{x}}^0 = (\boldsymbol{x}^0,\boldsymbol{u}(0))$ and the prime denoting differentiation with respect to the argument. The QSSA is satisfied by $\boldsymbol{u}' = 0$, however, this is not a meaningful approximation since $\boldsymbol{u}$ is not constant. In fact, it is precisely the dynamics driven by the oscillations in $\boldsymbol{u}$ that we are interested in exploring. Thus (2) is, from the perspective of the asymptotic limit as $\varepsilon \to 0$, an extension of problem (1).

Problem (2) is inherently multiscale, and thus brings with it all the challenges discussed. However, it differs structurally from the singularly perturbed problem (1). In (1) there are two sets of processes (fast and slow) acting separately in different intervals in time, whereas in (2) there are two sets of processes acting simultaneously in time [16]. The theory developed here is primarily focused on the response to exogenous oscillations, and therefore does not delve into the geometry of the invariant manifolds of the dynamics [18]. It is this observation that allows the treatment to be fairly generic and thus widely applicable.

One approach to problem (2) is to appeal to the intuition that the system effectively responds to an average of the periodically oscillating signal, and $\boldsymbol{u}(t/\varepsilon)$ may be replaced by its average over a period, which we denote $\overline{\boldsymbol{u}}$. This intuitive approximation satisfies the QSSA since $\overline{\boldsymbol{u}}$ does not vary in time. However, as before, it is unintuitive how to systematically improve the approximation accuracy, or obtain an estimate for the approximation error. This is particularly vexing in the context of problem (2), because it is the system response to the high-frequency component that we are primarily interested in exploring, which is lost in replacing $\boldsymbol{u}(t/\varepsilon)$ by $\overline{\boldsymbol{u}}$.

In this paper, we employ the method of multiple scales, whereby a new independent time variable is introduced to capture the fast-timescale variations occurring periodically alongside the slow-timescale variations. Similarly to the method of matched asymptotic expansions, the solution is expressed as an asymptotic expansion and thus allows higher-order corrections and formal error estimates to be obtained systematically. It transpires that, when the system dynamics occur exclusively on the slow timescale, the leading-order contribution is nothing other than the intuitive suggestion to replace $\boldsymbol{u}(t/\varepsilon)$ by its average $\overline{\boldsymbol{u}}$. By recognising the intuitive reasoning as the dominant term in a systematic analytical framework, we obtain both a stronger justification for the intuition, as well as a systematic method to improve upon it. Of particular interest is the common case where the timescale separation is not sufficiently near infinity for the leading-order term to provide an adequate estimate. Our focus in this case is on revealing the higher-order structure of the dynamics.

For further discussion regarding asymptotic techniques, including matched asymptotics for singularly perturbed problems as well as the method of multiple scales, we refer the reader to Refs. [16, 22, 23]. Alternative approaches, such as the method of averaging, are expounded upon in Ref. [24]. A more comprehensive historical perspective is provided in Ref. [25].

The multiple-scales approach has been employed previously in biochemical modeling,

for example, to capture limit-cycle behaviour in gene regulatory networks [26]. However, as we demonstrate in Section 4, in the context of oscillatory inputs contemporary work has either not identified the utility of this tool or has avoided its use for other reasons. We seek to remedy this by outlining the approach in an accessible yet generic derivation. We provide examples designed to allow the reader to accumulate a solid grasp of the algebra while simultaneously developing an intuition for how the calculations relate to the underlying biophysical process. By emphasising higher-order corrections, the presentation is mathematically comprehensive and practically more broadly applicable. Ultimately, our hope is that this contributes to demystifying the multiple-scales approach and encouraging its wider use.

The remainder of the paper is organised as follows. In Section 2, we discuss the general approach to the nonlinear case, and make further process in the affine case. The class of linear systems (included in the affine case) is of particular importance, since it includes the chemical master equation [27, 28] and its continuum approximations [13, 29, 30]. In Section 3 we demonstrate three examples of applying the framework to different affine problem structures: a scalar ordinary differential equation, a continuous-time Markov process governed by a master equation (that is, a system of coupled ordinary differential equations), and a Fokker–Planck partial differential equation. In Section 4, we tackle a system considered in the literature modeling the expression of a gene of interest by an optogenetic transcription factor. We show how the multiple-scales approach is applied to a nonlinear fast–slow system. Our analysis reveals key scaling laws and yields insights that allow us to clarify and simplify the requisite assumptions, as well as extend the scope of previous results. Finally, in Section 5 we discuss and summarise our findings.

2. High-frequency oscillatory input

2.1. The general nonlinear case

Our aim is to systematically derive the multiple-scales approximation of (2). We begin by tackling a general nonlinear case, and progressively add more structure which we leverage to obtain increasingly tractable problems. The goal of this stepwise approach is, on the one hand, to demonstrate that the method is applicable to an incredibly general class of problems requiring very few assumptions a priori. On the other hand, the most general setting remains somewhat intractable, therefore, adding additional structure in a stepwise fashion clarifies the gain of each additional assumption.

We set out by considering $\boldsymbol{y}$, $\boldsymbol{x}$, and $\boldsymbol{u}$ to be vector-valued functions of time, of dimensions M, N and K, respectively. We consider a general operator setting where the right-hand sides $\boldsymbol{f}$ and $\boldsymbol{g}$ may both depend on, and act on, spatial dimensions of $\boldsymbol{y}$ and $\boldsymbol{x}$ if present, denoting the spatial dimension by ℓ. We assume appropriate boundary conditions are prescribed where necessary. This formulation allows us to capture nonlinear systems of ODEs, PDEs, integral equations, etc., thereby demonstrating the generality of the multiple-scales approach for fast–slow systems of the form (2).

We assume that the characteristic system response time is of order unity, while the input signal $\boldsymbol{u}(t/\varepsilon)$ is of a high-frequency periodic form, with period ε for some $\varepsilon \ll 1$. We exploit this separation of timescales by a multiple-scales asymptotic expansion [16], which entails introducing the fast timescale $\tau = t/\varepsilon$ on which the high-frequency periodic variations of $\boldsymbol{u}$ are resolved, and writing the solution as a function of both the slow and the fast timescales, $\boldsymbol{y}(t,\tau)$ and $\boldsymbol{x}(t,\tau)$. Two key assumptions accompany the introduction of τ. First, we treat the fast timescale τ to be independent of the original timescale t. These scales are not strictly independent, nevertheless, it proves to be a powerful assumption as it allows for significant

decoupling in the analysis. Second, we assume that the solution is periodic with respect to τ. This assumption is required to constrain the additional freedom introduced by the independent fast timescale. The multiple-scales transformation involves replacing the differential operator in time via

$$\frac{\mathrm{d}}{\mathrm{d}t} \mapsto \frac{\partial}{\partial t} + \frac{1}{\varepsilon}\frac{\partial}{\partial \tau}, \tag{3}$$

which, upon application to (2), yields the system

$$\frac{\partial \boldsymbol{y}}{\partial t} + \frac{1}{\varepsilon}\frac{\partial \boldsymbol{y}}{\partial \tau} = \boldsymbol{f}(\boldsymbol{y},\boldsymbol{x},\boldsymbol{u}(\tau),t), \qquad \boldsymbol{y}|_{t=0} = \boldsymbol{y}^0, \tag{4a}$$

$$\varepsilon\frac{\partial \boldsymbol{x}}{\partial t} + \frac{\partial \boldsymbol{x}}{\partial \tau} = \boldsymbol{g}(\boldsymbol{y},\boldsymbol{x},\boldsymbol{u}(\tau),t), \qquad \boldsymbol{x}|_{t=0} = \boldsymbol{x}^0. \tag{4b}$$

Implicitly, we assume that all the high-frequency input is captured in $\boldsymbol{u}(\tau)$.

Seeking an asymptotic solution of (4) in the limit as $\varepsilon \to 0$, we pose power series expansions in ε,

$$\boldsymbol{y} \sim \boldsymbol{y}_0 + \varepsilon\boldsymbol{y}_1 + \cdots, \qquad \boldsymbol{x} \sim \boldsymbol{x}_0 + \varepsilon\boldsymbol{x}_1 + \cdots. \tag{5}$$

The asymptotic solution is obtained by substituting (5) into (4) and collecting terms of matching order in ε and ensuring equality at each order. While a power series expansion does not capture every perturbation structure [16], for the sake of simplicity we assume this typical case. To this end, we need to expand the right-hand sides asymptotically with respect to ε. It is convenient to consider the vector combining the state variables and their spatial derivatives

$$\boldsymbol{z} := (\boldsymbol{y},\boldsymbol{x}), \tag{6}$$

which inherits the expansion

$$\boldsymbol{z} \sim \boldsymbol{z}_0 + \varepsilon\boldsymbol{z}_1 + \cdots. \tag{7}$$

Temporarily suppressing the dependence on $\boldsymbol{u}(\tau)$ and t, we formally Taylor expand $\boldsymbol{f}(\boldsymbol{z})$ to find that

$$\boldsymbol{f}(\boldsymbol{z}) \sim \sum_{i=0}^{\infty} \frac{\varepsilon^i}{i!}\left[\left.\frac{\mathrm{d}^i \boldsymbol{f}(\boldsymbol{z})}{\mathrm{d}\varepsilon^i}\right|_{\varepsilon=0}\right] = \sum_{i=0}^{\infty} \varepsilon^i \boldsymbol{F}_i(\boldsymbol{z}_0,\ldots,\boldsymbol{z}_i), \tag{8}$$

for some $\boldsymbol{F}_i$ that, crucially, depend only on $\{\boldsymbol{z}_k\}_{k=0}^{i}$. Similarly, the expansion of $\boldsymbol{g}(\boldsymbol{z})$ takes the form

$$\boldsymbol{g}(\boldsymbol{z}) \sim \sum_{i=0}^{\infty} \varepsilon^i \boldsymbol{G}_i(\boldsymbol{z}_0,\ldots,\boldsymbol{z}_i). \tag{9}$$

Equipped with the asymptotic expansions (8) and (9), we may now determine the equations governing each order by collecting terms of matching powers of ε. Reintroducing the dependence on $\boldsymbol{u}(\tau)$ and t, we find that, for $i \geq 0$,

$$\frac{\partial \boldsymbol{y}_{i-1}}{\partial t} + \frac{\partial \boldsymbol{y}_i}{\partial \tau} = \boldsymbol{F}_{i-1}(\boldsymbol{z}_0,\ldots,\boldsymbol{z}_{i-1},\boldsymbol{u}(\tau),t), \qquad \boldsymbol{y}_i|_{t=0} = \boldsymbol{y}_i^0, \tag{10a}$$

$$\frac{\partial \boldsymbol{x}_{i-1}}{\partial t} + \frac{\partial \boldsymbol{x}_i}{\partial \tau} = \boldsymbol{G}_i(\boldsymbol{z}_0,\ldots,\boldsymbol{z}_i,\boldsymbol{u}(\tau),t), \tag{10b}$$

where any terms of index -1 are taken to be zero, and the solution is assumed periodic in τ. Employing the τ-periodicity, we integrate (10a) to find that

$$\frac{\mathrm{d}}{\mathrm{d}t}\int_0^1 \boldsymbol{y}_i(t,\tau)\,\mathrm{d}\tau = \int_0^1 \boldsymbol{F}_i(\boldsymbol{z}_0,\ldots,\boldsymbol{z}_i,\boldsymbol{u}(\tau),t)\,\mathrm{d}\tau. \tag{11}$$

We have not written an initial condition for $\boldsymbol{x}_i$ in (10b) since the τ-periodicity of the solutions precludes the fast variables $\boldsymbol{x}_i$ from satisfying an arbitrary initial condition.

At first glance, it is unclear whether (10) is closed: To determine $\boldsymbol{y}_j$ we need both its t and τ derivatives, which are governed by (10a) for $i = j, j+1$. However, for $i = j+1$, equation (10a) depends on $\boldsymbol{y}_{j+1}$. Therefore, it may seem that (10) constitutes an infinite family of coupled equations. As we now demonstrate, τ-periodicity is the crucial ingredient in being able to construct from (10) a hierarchy of closed equations.

We begin with the base case, $i = 0$, where (10) and (11) become

$$\frac{\partial \boldsymbol{y}_0}{\partial \tau} = 0, \tag{12a}$$

$$\frac{\partial \boldsymbol{x}_0}{\partial \tau} = \boldsymbol{G}_0(\boldsymbol{z}_0,\boldsymbol{u}(\tau),t), \tag{12b}$$

$$\frac{\mathrm{d}\boldsymbol{y}_0}{\mathrm{d}t} = \int_0^1 \boldsymbol{F}_0(\boldsymbol{z}_0,\boldsymbol{u}(\tau),t)\,\mathrm{d}\tau, \qquad \boldsymbol{y}_0(0) = \boldsymbol{y}_0^0. \tag{12c}$$

We see from (12a) that the leading-order slow variables $\boldsymbol{y}_0$ do not vary on the fast timescale τ, and the system (12b) and (12c) is closed with respect to $(\boldsymbol{y}_0,\boldsymbol{x}_0)$. We assume that system (12) is well posed, in that it admits a unique τ-periodic solution. In light of the uniqueness, we see that we cannot satisfy an arbitrary initial condition. We discuss the ramifications of this mismatch in further detail in Section 4.4 and Appendix A.

Having determined the governing equations for $\boldsymbol{y}_0$ and $\boldsymbol{x}_0$, we argue by induction that the remaining orders may be determined successively. Given $\{\boldsymbol{y}_j,\boldsymbol{x}_j\}_{j=0}^{i-1}$, it follows from (10a) that

$$\frac{\partial \boldsymbol{y}_i}{\partial \tau} = \boldsymbol{F}_{i-1}(\boldsymbol{z}_0,\ldots,\boldsymbol{z}_{i-1},\boldsymbol{u}(\tau),t) - \frac{\partial \boldsymbol{y}_{i-1}}{\partial t}, \qquad \boldsymbol{y}_i|_{t=0} = \boldsymbol{y}_i^0, \tag{13}$$

The right-hand side of equation (13) is a known function of t and τ, which may be integrated to give $\boldsymbol{y}_i$

$$\boldsymbol{y}_i(t,\tau) = \boldsymbol{c}_i(t) + \int_0^\tau \boldsymbol{F}_{i-1}(\boldsymbol{z}_0(t,s),\ldots,\boldsymbol{z}_{i-1}(t,s),\boldsymbol{u}(s),t) - \frac{\partial \boldsymbol{y}_{i-1}}{\partial t}(t,s)\,\mathrm{d}s, \tag{14}$$

where $\boldsymbol{c}_i(t)$ is a constant of integration with respect to τ, in other words, an arbitrary function of t (and possibly space). It then follows from (10b) and (11) that

$$\begin{aligned}\frac{\mathrm{d}\boldsymbol{c}_i}{\mathrm{d}t} = &\int_0^1 \boldsymbol{F}_i(\boldsymbol{z}_0,\ldots,\boldsymbol{z}_i,\boldsymbol{u}(\tau),t)\,\mathrm{d}\tau \\ &- \frac{\mathrm{d}}{\mathrm{d}t}\int_0^1\int_0^\tau \boldsymbol{F}_{i-1}(\boldsymbol{z}_0(t,s),\ldots,\boldsymbol{z}_{i-1}(t,s),\boldsymbol{u}(s),t) - \frac{\partial \boldsymbol{y}_{i-1}}{\partial t}(t,s)\,\mathrm{d}s\,\mathrm{d}\tau,\end{aligned} \tag{15a}$$

$$\boldsymbol{c}_i(0) = \boldsymbol{y}_i^0, \tag{15b}$$

$$\frac{\partial \boldsymbol{x}_i}{\partial \tau} = \boldsymbol{G}_i(\boldsymbol{z}_0,\ldots,\boldsymbol{z}_i,\boldsymbol{u}(\tau),t) - \frac{\partial \boldsymbol{x}_{i-1}}{\partial t}. \tag{15c}$$

System (15) is closed, and, with the assumption that $\boldsymbol{x}_i$ is τ-period, we assume it is well posed. Note that (11), which is satisfied by imposing (15a), ensures that $\boldsymbol{y}_i$ is τ-periodic. This concludes the induction.

To recap, we have shown that, under very general assumptions on the system (2), the multiple-scales approach produces a closed system of equations that may be computed to arbitrary order. This calculation pertains to linear and nonlinear systems of ODEs, PDEs, integral equations, and so forth. For a more explicit formulation we need to impose more system structure. One case of great importance that we now pursue is the case of operators biaffine in the state and the oscillations.

2.2. The biaffine case

To make further progress, we consider the case where $\boldsymbol{f}$ and $\boldsymbol{g}$ contain contributions that are biaffine with respect to the state and the oscillations. By "biaffine", we refer to operators f and g of the forms

$$\begin{aligned}\boldsymbol{f}(\boldsymbol{z},\boldsymbol{u},t) &= \boldsymbol{F}^0(t)+\boldsymbol{F}^z(t)\boldsymbol{z}+\sum_{j=1}^{K} u^j\boldsymbol{F}_j^{uz}(t)\boldsymbol{z}+u^j\boldsymbol{F}_j^u(t),\\ \boldsymbol{g}(\boldsymbol{z},\boldsymbol{u},t) &= \boldsymbol{G}^0(t)+\boldsymbol{G}^z(t)\boldsymbol{z}+\sum_{j=1}^{K} u^j\boldsymbol{G}_j^{uz}(t)\boldsymbol{z}+u^j\boldsymbol{G}_j^u(t),\end{aligned} \tag{16}$$

that is, with inhomogeneous, linear, and bilinear components, where we denote the scalar components of the oscillation by u^j, that is, $\boldsymbol{u}=(u^1,\dots,u^K)$. The linear operators $\boldsymbol{F}^z(t)$ and $\boldsymbol{F}_j^{uz}(t)$ map the state $\boldsymbol{z}$ to vectors in $\mathbb{R}^M$ and may act on spatial dimensions of $\boldsymbol{z}$ (if these exist) and may depend (perhaps nonlinearly) on time t. The terms $\boldsymbol{F}^0(t),\boldsymbol{F}_j^u(t)\in\mathbb{R}^M$ may depend similarly on time. These comments pertain analogously to the $\boldsymbol{G}$ terms, after replacing the dimension M by N. For notational brevity we henceforth adopt the Einstein summation convention, where repeated unbound indices imply summation. This summation will always be over the components of $\boldsymbol{u}$, that is, from one to K.

The biaffine class is important because it encompasses many useful models. Indeed, many nonlinear models are well described locally by a linear form. One particularly important family of linear models captured within the present framework is the master equation and its continuum approximations. As alluded to in the name, the master equation is a universal description of a multitude of biological, chemical, physical, and social processes [27, 28, 31].

With the biaffine notation (16), we retrace our steps to find that the expansion terms $\boldsymbol{F}_i$ and $\boldsymbol{G}_i$ in (8) and (9) are given explicitly by the forms

$$\boldsymbol{F}_i = \left[\boldsymbol{F}^z+u^j\boldsymbol{F}_j^{uz}\right]\boldsymbol{z}_i+\mathbb{1}_{i=0}\left[\boldsymbol{F}^0+u^j\boldsymbol{F}_j^u\right], \tag{17a}$$

$$\boldsymbol{G}_i = \left[\boldsymbol{G}^z+u^j\boldsymbol{G}_j^{uz}\right]\boldsymbol{z}_i+\mathbb{1}_{i=0}\left[\boldsymbol{G}^0+u^j\boldsymbol{G}_j^u\right], \tag{17b}$$

where $\mathbb{1}_{i=0}$ is the indicator function, taking the value one for $i=0$ and zero otherwise. Armed with more specific forms for the coefficients $\boldsymbol{F}_i$ and $\boldsymbol{G}_i$, we rewrite the multiple-scales equations (10) as

$$\frac{\partial\boldsymbol{y}_{i-1}}{\partial t}+\frac{\partial\boldsymbol{y}_i}{\partial\tau} = \left[\boldsymbol{F}^z(t)+u^j(\tau)\boldsymbol{F}_j^{uz}(t)\right]\boldsymbol{z}_{i-1}+\mathbb{1}_{i-1=0}\left[\boldsymbol{F}^0(t)+u^j(\tau)\boldsymbol{F}_j^u(t)\right],\quad \boldsymbol{y}_i|_{t=0}=\boldsymbol{y}_i^0, \tag{18a}$$

$$\frac{\partial\boldsymbol{x}_{i-1}}{\partial t}+\frac{\partial\boldsymbol{x}_i}{\partial\tau} = \left[\boldsymbol{G}^z(t)+u^j(\tau)\boldsymbol{G}_j^{uz}(t)\right]\boldsymbol{z}_i+\mathbb{1}_{i=0}\left[\boldsymbol{G}^0(t)+u^j(\tau)\boldsymbol{G}_j^u(t)\right]. \tag{18b}$$

Turning to the leading order, equations (12) take the forms

$$\frac{\partial \boldsymbol{y}_0}{\partial \tau} = 0, \tag{19a}$$

$$\frac{\partial \boldsymbol{x}_0}{\partial \tau} = \left[\boldsymbol{G}^z(t) + u^j(\tau)\boldsymbol{G}^{uz}_j(t)\right]\boldsymbol{z}_0 + \boldsymbol{G}^0(t) + u^j(\tau)\boldsymbol{G}^u_j(t), \tag{19b}$$

$$\frac{\mathrm{d}\boldsymbol{y}_0}{\mathrm{d}t} = \int_0^1 \left[\boldsymbol{F}^z(t) + u^j(\tau)\boldsymbol{F}^{uz}_j(t)\right]\boldsymbol{z}_0(t,\tau)\,\mathrm{d}\tau + \boldsymbol{F}^0(t) + \overline{u^j}\boldsymbol{F}^u_j(t), \qquad \boldsymbol{y}_0(0) = \boldsymbol{y}^0_0, \tag{19c}$$

where a bar denotes the fast-time-average, defined for any function, say $a(\tau)$, by

$$\bar{a} := \int_0^1 a(\tau)\,\mathrm{d}\tau. \tag{20}$$

The leading-order slow variables depend only on t, and (19b) is linear in $\boldsymbol{x}_0$, for which well-posedness is well characterised in many forms. For example, with spatial derivatives up to second order we obtain a system of diffusion equations.

Equations (19) constitute a closed system governing the leading-order $\boldsymbol{y}_0$ and $\boldsymbol{x}_0$. We now turn our attention to the general ith order, $\boldsymbol{y}_i$ and $\boldsymbol{x}_i$ for $i \geq 1$. The governing equations (14) and (15) take the forms

$$\begin{aligned}\boldsymbol{y}_i(t,\tau) = \boldsymbol{c}_i(t) &+ \int_0^\tau \left[\boldsymbol{F}^z(t) + u^j(s)\boldsymbol{F}^{uz}_j(t)\right]\boldsymbol{z}_{i-1}(t,s) - \frac{\partial \boldsymbol{y}_{i-1}}{\partial t}(t,s)\,\mathrm{d}s \\ &+ \mathbb{1}_{i-1=0}\left[\tau\boldsymbol{F}^0(t) + U^j(\tau)\boldsymbol{F}^u_j(t)\right],\end{aligned} \tag{21a}$$

$$\begin{aligned}\frac{\mathrm{d}\boldsymbol{c}_i}{\mathrm{d}t} = &\int_0^1 \left[\boldsymbol{F}^z(t) + u^j(\tau)\boldsymbol{F}^{uz}_j(t)\right]\boldsymbol{z}_i(t,\tau)\,\mathrm{d}\tau - \mathbb{1}_{i-1=0}\left[\frac{\boldsymbol{F}^0(t)}{2} + \overline{U^j}\boldsymbol{F}^u_j(t)\right] \\ &- \frac{\mathrm{d}}{\mathrm{d}t}\int_0^1\int_0^\tau \left[\boldsymbol{F}^z(t) + u^j(s)\boldsymbol{F}^{uz}_j(t)\right]\boldsymbol{z}_{i-1}(t,s) - \frac{\partial \boldsymbol{y}_{i-1}}{\partial t}(t,s)\,\mathrm{d}s\,\mathrm{d}\tau,\end{aligned} \tag{21b}$$

$$\frac{\partial \boldsymbol{x}_i}{\partial \tau} = \left[\boldsymbol{G}^z(t) + u^j(\tau)\boldsymbol{G}^{uz}_j(t)\right]\boldsymbol{z}_i(t,\tau) - \frac{\partial \boldsymbol{x}_{i-1}}{\partial t}, \tag{21c}$$

$$\boldsymbol{c}_i(0) = \boldsymbol{y}^0_i, \tag{21d}$$

where $\overline{U^j}$ denotes the fast-time average of U^j the specific integral u^j from $\tau = 0$, given by

$$U^j(\tau) = \int_0^\tau u^j(s)\,\mathrm{d}s. \tag{22}$$

Ultimately, in the biaffine case, we have closed systems of equations governing all perturbations orders.

3. Slow dynamics with harmonic oscillations

In this section, we tackle the subclass of problems arising from the master equation and the Fokker–Planck continuum approximation, for example, that are linear in the state and affine in the oscillations. For the sake of a first demonstration, we consider the case of slow dynamics ($N = 0$ and $\boldsymbol{x}$ is absent from the system) linear with respect to the state. We thus retain the bilinear form $\boldsymbol{F}^{uz}$ and term linear in state only $\boldsymbol{F}^z$ from (16), but neither $\boldsymbol{F}^u$ nor $\boldsymbol{F}^0$. In the absence of fast variables, we may replace $\boldsymbol{z}$ by $\boldsymbol{y}$.

From (19) we see that the leading-order $\boldsymbol{y}_0$ remains independent of τ, with its t-dependence governed by

$$\frac{\mathrm{d}\boldsymbol{y}_0}{\mathrm{d}t} = \left[\boldsymbol{F}^z(t) + \overline{u^j}\boldsymbol{F}^{uz}_j(t)\right]\boldsymbol{y}_0(t), \qquad \boldsymbol{y}_0(0) = \boldsymbol{y}^0_0, \tag{23}$$

The ith order term (21) may be written, for $i \geq 1$, as

$$\boldsymbol{y}_i(t,\tau) = \boldsymbol{c}_i(t) + \int_0^\tau \left[\boldsymbol{F}^z(t) + u^j(s)\boldsymbol{F}^{uz}_j(t)\right]\boldsymbol{y}_{i-1}(t,s) - \frac{\partial \boldsymbol{y}_{i-1}}{\partial t}(t,s)\,\mathrm{d}s, \tag{24a}$$

where $\boldsymbol{c}_i$ is determined by

$$\begin{aligned}\frac{\mathrm{d}\boldsymbol{c}_i}{\mathrm{d}t} &= \int_0^1 \left[\boldsymbol{F}^z(t) + u^j(\tau)\boldsymbol{F}^{uz}_j(t)\right]\boldsymbol{y}_i(t,\tau)\,\mathrm{d}\tau \\ &\quad - \frac{\mathrm{d}}{\mathrm{d}t}\int_0^1\int_0^\tau \left[\boldsymbol{F}^z(t) + u^j(s)\boldsymbol{F}^{uz}_j(t)\right]\boldsymbol{y}_{i-1}(t,s) - \frac{\partial \boldsymbol{y}_{i-1}}{\partial t}(t,s)\,\mathrm{d}s\,\mathrm{d}\tau, \qquad (24b)\\ \boldsymbol{c}_i(0) &= \boldsymbol{y}^0_i. \qquad (24c)\end{aligned}$$

The leading-order dynamics (23) coincide with the intuition that the system is well approximated by the response to the averaged input signal since the oscillations appear only through their average $\overline{u^j}$. It follows that mean-preserving adjustments to the high-frequency component are lost: for example, for the scalar-valued $u(\tau) = \sin(2\pi\tau - \theta)$, we have $\bar{u} = 0$ irrespective of θ. Therefore, the mean is preserved independently of the phase, which may be undesirable if we hope to resolve the system response to the phase. Moreover, in general, the leading-order approximation suffers from an error of order $O(\varepsilon)$. When ε is small but not exceedingly so, the resulting errors can be particularly pronounced, requiring a more accurate approximation. Our aim is thus to demonstrate how the multiple-scales approach surpasses the simple intuition by capturing higher-order perturbations beyond the leading order, as in (24). In this case, the first-order contribution captures the dominant effect of the fluctuations on the system, and thus we calculate the first two orders, to yield the system response to fluctuations at an accuracy of $O(\varepsilon^2)$.

Before writing down the system governing the first two orders, we choose, for the examples in this section, a scalar oscillation ($K = 1$) given by the ε-periodic harmonic signal

$$u(\tau) = \sin(2\pi\tau - \theta). \tag{25}$$

The definite integral U and the fast-time averages are then given, respectively, by

$$U(\tau) = \frac{1}{2\pi}\left(\cos\theta - \cos(2\pi\tau - \theta)\right), \tag{26a}$$

and

$$\bar{u} = \overline{Uu} = 0, \qquad \overline{U} = \frac{\cos\theta}{2\pi}. \tag{26b}$$

We assume that the initial condition contains only a leading-order contribution. Then, with the harmonic signal (25) and associated identities (26), the systems (23) and (24)

governing the leading- and first-order contributions take the simple form

$$\frac{\mathrm{d}\boldsymbol{y}_0}{\mathrm{d}t} = \boldsymbol{F}^z(t)\boldsymbol{y}_0(t), \tag{27a}$$

$$\boldsymbol{y}_1(t,\tau) = \boldsymbol{c}_1(t) + U(\tau)\boldsymbol{F}^{uz}(t)\boldsymbol{y}_0(t), \tag{27b}$$

$$\frac{\mathrm{d}\boldsymbol{c}_1}{\mathrm{d}t} = \boldsymbol{F}^z(t)\boldsymbol{c}_1(t) + \boldsymbol{\mu}(t), \tag{27c}$$

$$\boldsymbol{\mu}(t) = \overline{U}\left[\boldsymbol{F}^z(t)\boldsymbol{F}^{uz}(t)\boldsymbol{y}_0(t) - \frac{\mathrm{d}}{\mathrm{d}t}\left[\boldsymbol{F}^{uz}(t)\boldsymbol{y}_0(t)\right]\right]. \tag{27d}$$

subject to the initial conditions

$$\boldsymbol{y}_0(0) = \boldsymbol{y}^0, \qquad \boldsymbol{c}_1(0) = \boldsymbol{0}. \tag{27e}$$

It follows from (27d) that $\boldsymbol{\mu} = \boldsymbol{0}$ for $\theta = (k+1/2)\pi$ and $k \in \mathbb{Z}$. This gives rise to a particularly straightforward first-order form: the first-order slow-scale contribution $\boldsymbol{c}_1$ is governed by the linear inhomogeneous equation (27c), but the inhomogeneity (27d) and initial condition (27e) are zero therefore so is $\boldsymbol{c}_1$. Thus, solving the leading-order problem suffices to give us the first-order contribution:

$$\boldsymbol{y}(t,\tau) \sim \boldsymbol{y}_0(t) + \varepsilon U(\tau)\boldsymbol{F}^{uz}(t)\boldsymbol{y}_0(t), \qquad \text{when} \qquad \boldsymbol{\mu} = \boldsymbol{0}. \tag{28}$$

This result may be generalised by writing the form of the first-order inhomogeneity $\boldsymbol{\mu}(t)$ in the general biaffine case of system (24) for arbitrary $\boldsymbol{u}$, where we find that

$$\boldsymbol{\mu} = \left[\overline{U^j} - \frac{\overline{u^j}}{2}\right]\boldsymbol{F}^z\boldsymbol{F}^{uz}_j\boldsymbol{y}_0 + \left[\overline{U^j u^k} - \frac{\overline{u^j}\,\overline{u^k}}{2}\right]\boldsymbol{F}^{uz}_k\boldsymbol{F}^{uz}_j\boldsymbol{y}_0 - \left[\overline{U^j} - \frac{\overline{u^j}}{2}\right]\frac{\mathrm{d}}{\mathrm{d}t}\left[\boldsymbol{F}^{uz}_j\boldsymbol{y}_0\right]. \tag{29}$$

It follows that, when the fast-time averages vanish $\overline{U^j} = \overline{u^j} = \overline{U^j u^k} = 0$ for all j and k, the asymptotic solution up to first order is given by

$$\boldsymbol{y}(t,\tau) \sim \boldsymbol{y}_0(t) + \varepsilon U^j(\tau)\boldsymbol{F}^{uz}_j(t)\boldsymbol{y}_0(t), \qquad \text{when} \qquad \overline{U^j} = \overline{u^j} = \overline{U^j u^k} = 0 \text{ for all } j,k. \tag{30}$$

Alternatively, we may obtain the result (30) when $\overline{u^j} = \overline{U^j u^k} = 0$ for all j and k (but $\overline{U^j}$ need not vanish) if it is also the case that, for all j, $\boldsymbol{F}^z$ commutes with $\boldsymbol{F}^{uz}_j$ and the latter is time-invariant. To see this, note that the time derivative commutes with $\boldsymbol{F}^{uz}_j$, and substitute (27a) into (29).

3.1. Oscillating growth rate

Our first example employs the scalar equation

$$\dot{p} = (\alpha + \beta u(t/\varepsilon))p, \qquad p(0) = p^0, \tag{31}$$

with the harmonic u given in (25), which could model growth in the presence of an oscillating environment, such as daily temperature or light variations, or seasonal water temperature. We find an analytical solution by using the integration factor $\mathrm{e}^{-\int^t \alpha+\beta u(t/\varepsilon)\,\mathrm{d}t}$, to give

$$p = p^0 \exp\left(\alpha t + \beta\varepsilon U(t/\varepsilon)\right), \tag{32}$$

for U defined in (26a). For the purpose of later comparison, we expand the exact solution (32) asymptotically with respect to ε:

$$p \sim p^0 \mathrm{e}^{\alpha t} \left(1 + \varepsilon\beta U(\tau) + O(\varepsilon^2)\right). \tag{33}$$

We now seek a multiple-scales solution, by rewriting equation (31) in the form of system (27). The state is scalar ($M = 1$) with no spatial dimension ($\ell = 0$), and the operators take the forms

$$F^{uz} = \beta, \qquad F^{z} = \alpha. \tag{34}$$

From (27a) we find that the leading-order term p_0 satisfies

$$\frac{\mathrm{d}p_0}{\mathrm{d}t} = \alpha p_0, \qquad p_0(0) = p^0, \tag{35}$$

and thus is given by

$$p_0 = p^0 \mathrm{e}^{\alpha t}. \tag{36}$$

The scalar-multiplication operators (34) commute and are time-invariant. It follows from (30) that the multiple-scales solution is given by

$$p \sim p^0 \mathrm{e}^{\alpha t} \left(1 + \varepsilon\beta U(\tau)\right) + O(\varepsilon^2). \tag{37}$$

We see that the form (37) matches the expansion of the exact solution (33).

We compare the exact solution (solid curves) to the multiple-scales asymptotic approximation (dashed curves) in Fig. 1 for varying system and input parameters α, β, θ, ε. In Fig. 1a we see how different base growth rates α manifest in the presence of oscillations. We observe that the oscillations are proportional to the magnitude of p and, similarly, the asymptotic error appears in the same proportion (Fig. 1a inset). The agreement is excellent even though the value of $\varepsilon = 0.5$ is moderate. In Fig. 1b the oscillations and the error increase with β. The discrepancy appears large despite the smaller value of ε because the vertical scale is less extensive. In Fig. 1c we see the comparison for different oscillation time-delays θ. The agreement is best for $\theta = \pi/2$, which is the value for which $\overline{U} = 0$ leading to some higher-order inhomogeneities to vanish. Finally, we see in Fig. 1d how increasing ε increases the period and the error. Interestingly, the maximal error occurs consistently at the oscillation extrema.

3.2. Master equation of discrete system

Consider a continuous-time Markov chain with two states. The propensity to transition from the first to the second state is $\alpha - u(t/\varepsilon)$, while from second to first is $\beta + u(t/\varepsilon)$, for the harmonic u in (25). For non-negative propensities, we require $\alpha, \beta \geq 1$. The signal u represents an additional bias of transitioning to, and remaining in, the first state. The master equation, governing the probability distribution of being in either state, is given by

$$\frac{\mathrm{d}\boldsymbol{p}}{\mathrm{d}t} = \begin{pmatrix} -\alpha + u(t/\varepsilon) & \beta + u(t/\varepsilon) \\ \alpha - u(t/\varepsilon) & -\beta - u(t/\varepsilon) \end{pmatrix} \boldsymbol{p}, \qquad \boldsymbol{p}(0) = \boldsymbol{p}^0. \tag{38}$$

The matrix on the right-hand side of (38) and its time-integral do not commute, and therefore the solution is not given by the matrix exponential. We may, however, solve this system

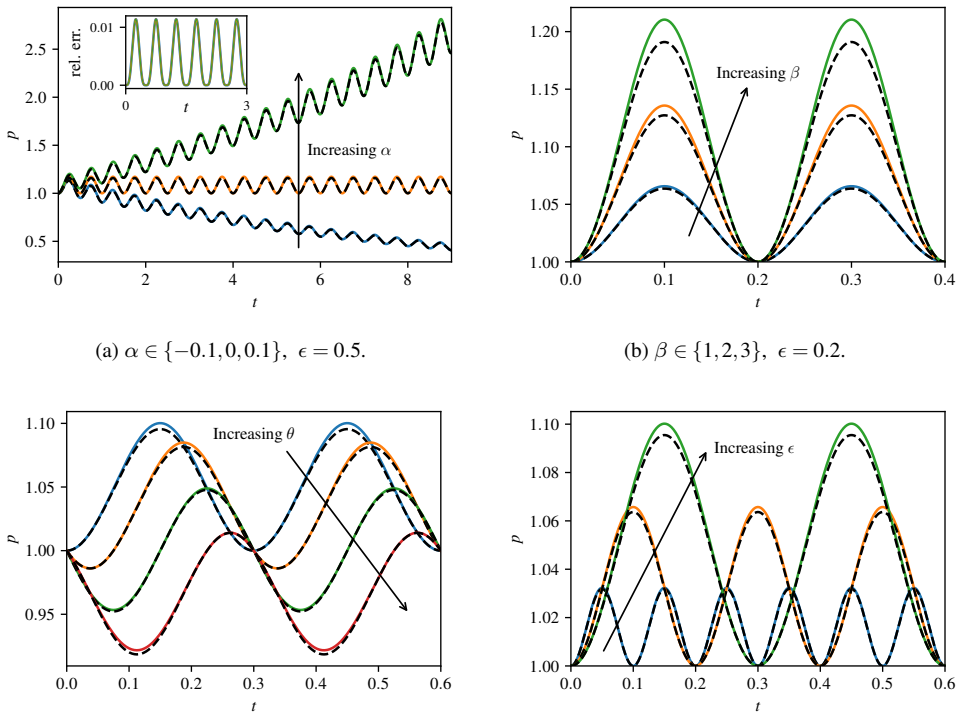

(a) $\alpha \in \{-0.1, 0, 0.1\},\ \epsilon = 0.5.$

(b) $\beta \in \{1, 2, 3\},\ \epsilon = 0.2.$

(c) $\theta \in \{0, \pi/4, \pi/2, 3\pi/4\},\ \epsilon = 0.3.$

(d) $\epsilon \in \{0.1, 0.2, 0.3\}.$

Figure 1. The solution (32) (solid curves) and multiple-scales approximation (37) (dashed curves) of the oscillating growth rate equation (31) for different unperturbed growth rates α, oscillation magnitudes β, timescale separation and oscillation period ε, and oscillation shifts θ. When unspecified, the parameters used are $\alpha = 0$, $\beta = 1$, $\theta = 0$, $p^0 = 1$. The inset in (a) depicts the relative error of the multiple-scales approximation for each value of α in the main plot (the curves are coloured correspondingly but lie exactly on top of one another making them indistinguishable).

by order reduction. From the conservation of total probability, we know that $(1,1)^\top \boldsymbol{p}(t) = (1,1)^\top \boldsymbol{p}^0 = 1$. Therefore, the second entry may be expressed as a function of the first, $\boldsymbol{p} = (p, 1-p)^\top$, whereby the system reduces to the scalar equation

$$\frac{\mathrm{d}p}{\mathrm{d}t}(t) = (-\alpha + u(t/\varepsilon))p(t) + (\beta + u(t/\varepsilon))(1 - p(t)), \tag{39}$$

which may be integrated by means of the integrating factor $\mathrm{e}^{(\alpha+\beta)t}$ to give

$$p(t) = \mathrm{e}^{-(\alpha+\beta)t}\left(p^0 + \int_0^t (\beta + u(s/\varepsilon))\,\mathrm{e}^{(\alpha+\beta)s}\,\mathrm{d}s\right). \tag{40}$$

Using the specific form for u in (25), we may calculate the integral on the right-hand side of (40) by parts to yield

$$p(t) = p^0 \mathrm{e}^{-(\alpha+\beta)t} + \frac{\beta}{\alpha+\beta}\left(1-\mathrm{e}^{-(\alpha+\beta)t}\right) + \frac{(\alpha+\beta)\left[\sin(2\pi t/\varepsilon-\theta)+\mathrm{e}^{-(\alpha+\beta)t}\sin\theta\right] - (2\pi/\varepsilon)\left[\cos(2\pi t/\varepsilon-\theta)-\mathrm{e}^{-(\alpha+\beta)t}\cos\theta\right]}{(2\pi/\varepsilon)^2+(\alpha+\beta)^2}. \tag{41}$$

For later comparison, we expand solution (41) asymptotically with respect to ε to give

$$p \sim p^0 \mathrm{e}^{-(\alpha+\beta)t} + \frac{\beta}{\alpha+\beta}\left(1-\mathrm{e}^{-(\alpha+\beta)t}\right) + \frac{\varepsilon}{2\pi}\left[\mathrm{e}^{-(\alpha+\beta)t}\cos\theta - \cos(2\pi t/\varepsilon-\theta)\right] + O(\varepsilon^2). \tag{42}$$

To pursue the multiple-scales approximation, we rewrite system (38) in the form of system (27), including two states ($M=2$) and no spatial dimensions ($\ell=0$), via

$$\boldsymbol{F}^{uz} = \begin{pmatrix} 1 & 1 \\ -1 & -1 \end{pmatrix}, \qquad \boldsymbol{F}^{z} = \begin{pmatrix} -\alpha & \beta \\ \alpha & -\beta \end{pmatrix}. \tag{43}$$

Following the prescribed recipe, the leading-order term governed by (27a) satisfies

$$\frac{\mathrm{d}\boldsymbol{p}_0}{\mathrm{d}t} = \boldsymbol{F}^z \boldsymbol{p}_0, \qquad \boldsymbol{p}(0) = \boldsymbol{p}^0, \tag{44}$$

which is solved (via the matrix exponential) by

$$\boldsymbol{p}_0(t) = \frac{1}{\alpha+\beta}\begin{pmatrix} \alpha\mathrm{e}^{-(\alpha+\beta)t}+\beta & \beta\left(1-\mathrm{e}^{-(\alpha+\beta)t}\right) \\ \alpha\left(1-\mathrm{e}^{-(\alpha+\beta)t}\right) & \alpha+\beta\mathrm{e}^{-(\alpha+\beta)t} \end{pmatrix}\boldsymbol{p}^0. \tag{45}$$

At the next order we determine $\boldsymbol{c}_1$ governed by (27c), which takes the form,

$$\frac{\mathrm{d}\boldsymbol{c}_1}{\mathrm{d}t} = \boldsymbol{F}^z\boldsymbol{c}_1 + \overline{U}(\boldsymbol{F}^z\boldsymbol{F}^{uz} - \boldsymbol{F}^{uz}\boldsymbol{F}^z)\boldsymbol{p}_0 = \boldsymbol{F}^z\boldsymbol{c}_1 + \overline{U}(\alpha+\beta)\begin{pmatrix} -1 \\ 1 \end{pmatrix}, \tag{46}$$

with zero initial conditions. Again exploiting the conservation property whereby $(1,1)^\top \boldsymbol{c}_1(t) = 0$ for all times, hence $\boldsymbol{c}_1(t) = (c_1(t), -c_1(t))^\top$, it suffices to solve only for the first component,

$$\frac{\mathrm{d}c_1}{\mathrm{d}t} = -(\alpha+\beta)c_1 - \overline{U}(\alpha+\beta), \tag{47}$$

which admits the solution $c_1(t) = -\overline{U}(1-\mathrm{e}^{-(\alpha+\beta)t})$. Combining (47) with the leading-order (45) via (27b), the asymptotic solution takes the form

$$\boldsymbol{p} \sim \frac{1}{\alpha+\beta}\begin{pmatrix} \alpha\mathrm{e}^{-(\alpha+\beta)t}+\beta & \beta\left(1-\mathrm{e}^{-(\alpha+\beta)t}\right) \\ \alpha\left(1-\mathrm{e}^{-(\alpha+\beta)t}\right) & \alpha+\beta\mathrm{e}^{-(\alpha+\beta)t} \end{pmatrix}\boldsymbol{p}^0 + \varepsilon\left[U(\tau) - \overline{U}(1-\mathrm{e}^{-(\alpha+\beta)t})\right]\begin{pmatrix} 1 \\ -1 \end{pmatrix} + O(\varepsilon^2), \tag{48}$$

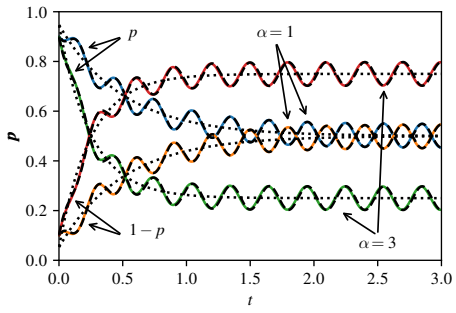

Figure 2. The solution (41) (solid curves) and multiple-scales approximation (48) (dashed curve) of the master equation (38) governing the probability to be in either of the two system states $\boldsymbol{p} = (p, 1-p)$, with a transition rate of $\alpha - u(t/\varepsilon)$ from the first state to the second, and a transition rate of $\beta + u(t/\varepsilon)$ from the second state to the first, where u is given in (25). We set $\beta = 1$, the oscillation parameters $\varepsilon = 0.3$, $\theta = 0$, and the initial conditions $\boldsymbol{p}^0 = (0.9, 0.1)$. The dotted curves show the fast-time-averaged first-order quantity (49).

which, using (26), we see is in agreement with the asymptotic expansion of the exact solution (42).

In Fig. 2 we compare the exact solution (solid curves) and the multiple-scales approximation (dashed curves) for $\beta = 1$ and two values of the base transition rate α. We find excellent agreement with the moderate value of $\varepsilon = 0.3$. The long-time behaviour of the base process (i.e. in the absence of oscillations, $u \equiv 0$) is to converge to being in the states with probabilities proportional to the incoming transition rate, that is, being in the first state with probability $\beta/(\alpha+\beta) = 1/(\alpha+1)$. When $\alpha = 1$, the base transition rates between the two states are equal, and the long-time behaviour is to converge to being in each state with equal probability. When $\alpha = 3$, we expect convergence to $\boldsymbol{p} \to (1/4, 3/4)$. This behaviour is observed in Fig. 2, along with the variations driven by the oscillations.

We conclude this example with two observations. First, the behaviour of the system in the absence of oscillations is described by the leading-order dynamics. We might then expect the first-order contribution to have zero mean on the fast timescale, however, we see that this is not in general the case. In the present example, integrating the asymptotic expansion in (48) we find that

$$\int_\tau^{\tau+1} \boldsymbol{p}(t,s)\,\mathrm{d}s \sim \boldsymbol{p}_0(t) + \varepsilon \overline{U}\, \mathrm{e}^{-(\alpha+\beta)t} \begin{pmatrix} 1 \\ -1 \end{pmatrix} + O(\varepsilon^2). \tag{49}$$

We deduce that the oscillations have an $O(\varepsilon)$ effect on the process, even once the oscillations have been averaged out. It might be tempting to postulate that this contribution always decays, as in (49). However, as we can see from the previous example in Section 3.1, after averaging the oscillations may still contribute to the coefficient of the leading-order terms. This further demonstrates the importance of resolving the higher-order terms for moderate values of ε.

Second, we have kept the first two examples simple enough to be able to solve explicitly, to provide an analytical comparison to the multiple-scales approximation. However, most applications involve systems of far greater complexity that cannot be solved exactly, although the multiple-scales system remain tractable. Observe how in this example the exact solution was only obtainable in closed form by calculating the integral (40) by parts for the harmonic form of u. While this step does not easily generalise (and would require a direct asymptotic analysis of the integral in more general cases), the multiple-scales solution (48) never required

the harmonic form of u and thus retains generality. Similarly, while the original equation (38) is not solvable by matrix exponentiation, the multiple-scales problems are time-invariant and therefore straightforward to solve by exponentiation. This time invariance is a direct consequence of the separation of scales: the multiple-scales ansatz encapsulated the timescale separation, which renders the constitutive systems time-invariant.

We now proceed to an example where we are not in possession of an exact solution, but where the multiple-scales approximation still provides us with a wealth of analytical insight.

3.3. Fokker–Planck PDE for continuum state

Consider the continuous birth–death process with an oscillating birth rate $b+u(t/\varepsilon)$, for the harmonic u in (25), and constant death rate d proportional to the population size, represented by the continuum state variable x. The distribution $p(x,t)$ over state and time is governed by the Fokker–Planck equation

$$\frac{\partial}{\partial t}p(x,t) = -\frac{\partial}{\partial x}[(b+u(t/\varepsilon)-dx)p(x,t)] + \frac{1}{2\Omega}\frac{\partial^2}{\partial x^2}[(b+u(t/\varepsilon)+dx)p(x,t)], \tag{50a}$$

$$p(x,0) = p^0(x), \tag{50b}$$

on the domain $(x,t)\in[0,\infty)^2$ with zero-flux and vanishing far-field boundary conditions

$$\left(-b-u(t/\varepsilon)+\frac{d}{2\Omega}\right)p(0,t) + \frac{b+u(t/\varepsilon)}{2\Omega}\frac{\partial p}{\partial x}(0,t) = 0, \tag{50c}$$

$$p\to 0 \text{ as } x\to\infty. \tag{50d}$$

The parameter Ω quantifies the characteristic size of the system, and, while typically large, the stochastic contribution described by the diffusive term of magnitude $O(1/\Omega)$ cannot be neglected as it is a singular perturbation [32].

We may write (50) in the multiple-scales form of (27). The equation is scalar ($M=1$) and contains spatial derivatives up to second order ($\ell=2$) where the operators take the forms

$$F^{uz}p(x,t) = -\frac{\partial p}{\partial x} + \frac{1}{2\Omega}\frac{\partial^2 p}{\partial x^2}, \tag{51}$$

$$F^{z}p(x,t) = -\frac{\partial}{\partial x}[(b-dx)p(x,t)] + \frac{1}{2\Omega}\frac{\partial^2}{\partial x^2}[(b+dx)p(x,t)]. \tag{52}$$

The now familiar asymptotic procedure finds the leading-order contribution governed by (27a) in the form

$$\frac{\partial p_0}{\partial t} = F^z p_0, \qquad\qquad p_0(x,0) = p^0(x), \tag{53a}$$

subject to the boundary conditions

$$\left(-b+\frac{d}{2\Omega}\right)p_0(0,t) + \frac{b}{2\Omega}\frac{\partial p_0}{\partial x}(0,t) = 0, \qquad\qquad p_0\to 0 \text{ as } x\to\infty. \tag{53b}$$

The first-order contribution p_1 is given by (27b), for c_1 satisfying (27c) which takes the form

$$\frac{\partial c_1}{\partial t}(x,t) = F^z c_1(x,t) + \overline{U}(F^z F^{uz} - F^{uz}F^z)p_0(x,t), \tag{54a}$$

subject to the boundary conditions

$$\left(-b+\frac{d}{2\Omega}\right)p_1(0,t)+\frac{b}{2\Omega}\frac{\partial p_1}{\partial x}(0,t)=0, \qquad c_1\to 0 \text{ as } x\to\infty. \tag{54b}$$

We do not know how to solve the original equation (50) analytically, and instead choose to approximate it numerically using the Flips solver [33]. On the other hand, the problems (53) and (54) are separable, and we could seek to solve the associated eigenvalue problem. However, the calculations reduce to solving the confluent hypergeometric differential equation with many details that detract from the central idea. Many other asymptotic limits of the problem are more straightforward. We choose to consider the large-time asymptotics of (53) and (54), where the t-derivatives are negligible leaving steady state problems. Importantly, the τ-variations are retained, and so the time variations driven by the high-frequency input are still captured.

We may solve the steady version of (53) by integrating once, and imposing the zero-flux boundary condition, to obtain

$$-(b-dx)p_0(x)+\frac{1}{2\Omega}\frac{\mathrm{d}}{\mathrm{d}x}[(b+dx)p_0(x)]=0. \tag{55}$$

Rearranging, we find that

$$\frac{\mathrm{d}}{\mathrm{d}x}\log[(b+dx)p_0(x)]=2\Omega\frac{b-dx}{b+dx}, \tag{56}$$

from which it follows that the solution is given by

$$p_0(x)=c\,\mathrm{e}^{-2\Omega x}(b+dx)^{(4b\Omega/d)-1}, \tag{57}$$

for a constant of integration c.

Since the steady form of (53) is $F^z p_0=0$, the steady first-order problem (54) takes the form $F^z[c_1+\overline{U}F^{uz}p_0]=0$, and admits the solution

$$c_1=-\overline{U}F^{uz}p_0. \tag{58}$$

The solution (58) satisfies the boundary conditions since p_0 captures identically zero flux, therefore, $p_1=c_1+U(\tau)F^{uz}p_0=(U(\tau)-\overline{U})F^{uz}p_0$ inherits this property, as the flux operator and F^{uz} commute. Using (55) and (57), p_1 may be written as

$$p_1(x,\tau)=-c(U(\tau)-\overline{U})\frac{\mathrm{d}}{\mathrm{d}x}\left[\mathrm{e}^{-2\Omega x}(b+dx)^{(4b\Omega/d)-2}\left(2dx+\frac{d}{2\Omega}\right)\right]. \tag{59}$$

Ultimately, we arrive at the large-time approximation

$$p\sim p_0(x)+\varepsilon\, p_1(x,\tau). \tag{60}$$

In Fig. 3 we plot the numerical solution (solid curves) for different initial conditions, and note how they do indeed converge to the asymptotic regime in (60) in $O(1)$ time, exhibiting excellent agreement.

This example demonstrates a case where, despite a seemingly impenetrable problem, the multiple-scales approximation captures the timescale separation to produce separable equations that are significantly more tractable.

The examples in this section demonstrate the application of the multiple-scales approach to systems linear in the state whose dynamics are slow relative to the oscillations. We now turn our attention to a nonlinear system previously studied in the literature that includes fast species and show how our analysis may be leveraged to yield fresh insights. Our analysis quantifies the underlying assumptions of previous work, ties the experimental observations more concretely to the model, and crystalises the conclusions.

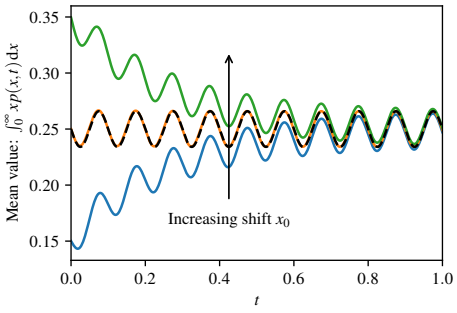

Figure 3. The numerical approximation (solid curves) and large-time multiple-scales approximation (60) (dashed curves) of the PDE (50a) governing the probability $p(x,t)$ that the birth–death process is of size x at time t. The birth rate is $b+u(t/\varepsilon)$ for the harmonic u given in (25), the death rate is d for $b=1$, $d=4$, the system size is $\Omega=100$, and the oscillation parameters are $\varepsilon=0.1$, $\theta=\pi/2$. The initial condition used for the simulation is given by the steady first-order asymptotic approximation (60) shifted by $x_0\in\{-0.1,0,0.1\}$, that is, $p(x,0)=p_0(x-x_0)+\varepsilon p_1(x-x_0,0)$.

Table 1. Parameter definitions and values from Ref. [34] for the model (61) for genetic constructs with five (5xBS-CYC180pr) and two (2xBS-CYC180pr) binding sites (BS) for the transcription factor (EL-222) upstream of a truncated CYC1 promoter driving the fluorescent protein expression.

Param.	**Description**	**5 BS**	**2 BS**	**Unit**
T_{tot}	Total transcription factor	2000	2000	—
k_{on}	Activation rate per light intensity	0.0016399	0.0016399	$\mathrm{min}^{-1}\,\mu\mathrm{W}^{-1}\,\mathrm{cm}^2$
k_{off}	Reversion rate	0.34393	0.34393	min^{-1}
k_{basal}	Basal transcription rate	0.02612	0.24358	min^{-1}
k_{max}	Max. induced transcription rate	13.588	11.031	min^{-1}
K	Transcription factor scale	956.75	1462.5	—
n	Hill coefficient	4.203	4.6403	—
k_{degR}	mRNA degradation rate	0.042116	0.042116	min^{-1}
k_{trans}	translation rate	1.4514	1.4514	min^{-1}
k_{degP}	Protein degradation rate	0.007	0.007	min^{-1}
v_{max}	Maximal light intensity	420	420	$\mu\mathrm{W}\,\mathrm{cm}^{-2}$
Λ	Pulse width	30	30	min

4. Case study: fast dynamics and nonlinearities

4.1. Model overview

In Ref. [34], a genetic construct is engineered in yeast cells to constitutively express the (inactive) transcription factor (TF) EL-222. Upon induction by light, the TF molecules dimerise (that is, two molecules join together to form a single construct), which forms the active TF and enables the transcription of the gene of interest. The transcription produces mRNA molecules from which the protein of interest may be expressed. We will outline the model and present the results obtained previously, which ultimately leverage a separation of timescales to achieve a particular biological outcome.

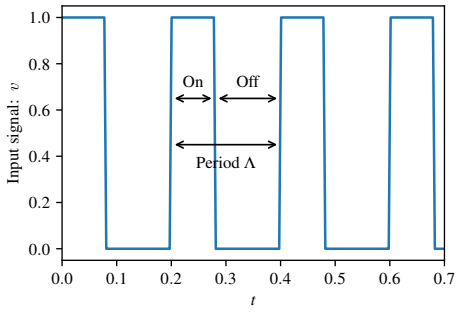

Figure 4. The rectangular waveform $v(t)$ given in (62) for $\Lambda = 0.2$ time units and $r = 0.4$. The duty cycle r is the fraction of each period the light is illuminated: On/Period.

The model is described by the system of ODEs

$$\frac{\mathrm{d}T}{\mathrm{d}t} = v_{\max} v(t) k_{\mathrm{on}} (T_{\mathrm{tot}} - T) - k_{\mathrm{off}} T, \tag{61a}$$

$$\frac{\mathrm{d}R}{\mathrm{d}t} = k_{\mathrm{basal}} + k_{\max} \frac{T^n}{K^n + T^n} - k_{\mathrm{degR}} R, \tag{61b}$$

$$\frac{\mathrm{d}P}{\mathrm{d}t} = k_{\mathrm{trans}} R - k_{\mathrm{degP}} P, \tag{61c}$$

where T, R, and P represent the concentrations of active TF, mRNA, and protein molecules, respectively. It is assumed that the total concentration of TF, denoted T_{tot}, remains constant on the timescale of interest. A light signal of maximal intensity $v_{\max}$, modulated by the profile $v(t) \in [0,1]$, serves to activate (i.e. dimerise) the inactive TF molecules at a rate per light intensity of k_{on} times the concentration of inactive TF. The activation is assumed to occur on a significantly faster than the timescales of interest. The transcription of mRNA molecules is described by a basal rate k_{basal}, in addition to the rate driven by the active TF, T, modulated by a Hill function, with coefficient n, scale K, and maximum rate $k_{\max}$. The protein in transcribed at a rate of k_{trans} times the mRNA concentration. The active TF deactivates at a rate k_{off}, while the mRNA and protein molecules degrade at rates k_{degR} and k_{degP} respectively. Parameter values derived from fitting experimental data in Ref. [34] are displayed in Table 1 for two variants of the promoter construct.

The experimentally measurable quantity is the concentration of the protein of interest after a long duration $t = t_f$. Practically, protein concentration is measured via fluorescence by flow cyctometry. With the parameters in Table 1, simulations exhibit good agreement with additional experimental results (see Ref. [34] for further details). One of the central outcomes is the comparison between two different light modulation profiles $v(t)$: amplitude modulate (AM) and pulse-width modulation (PWM). AM refers to choosing a fixed amplitude $v(t) \equiv v_0$ for the duration of the experiment, while PWM refers to using the pulsatile signal

$$v(t) = \sum_{i=-\infty}^{\infty} \mathbb{1}_{[0,r]} \left(\frac{t}{\Lambda} - i \right), \tag{62}$$

where $\mathbb{1}$ is the indicator function: $\mathbb{1}_{[0,1]}(x)$ takes the value one if $x \in [0,1]$, and zero otherwise. The profile (62) describes a periodic rectangular waveform with (dimensional) period Λ and pulse width $r\Lambda$ for $r \in [0,1]$ commonly referred to as the duty cycle (see Fig. 4).

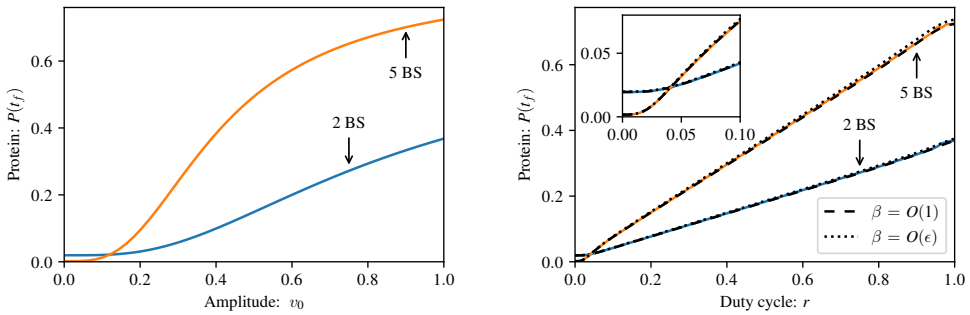

Figure 5. Dose–response curves in the **(a)** AM; **(b)** PWM regimes, for two sets of parameter values corresponding to different genetic constructs (see Table 1) for a terminal time of $t_f = 360k_{\text{degP}}$, which corresponds to 6 hours. Solid curves show full numerical solutions of system (67), while broken curves show the leading-order multiple-scale approximation governed by (B.3) and (B.26) for two different choices of β scale, and using the exponentially-accurate T_0 given in (A.2). Pulse-width modulation exhibits a nearly linear response and is in good agreement to both asymptotic approximations. The inset in (b) shows a close-up for small r, where the deviation from the affine profile is visible.

It may be shown that the AM results in nonlinear dose–response curves (Fig. 5a), while for a carefully chosen period Λ, the dose–response curves are nearly linear (Fig. 5b). Linear response curves allow for the construction of genetic circuits that demonstrate particular phenotypes through coordinated multi-gene expression [34]. Intuitively, the pulse timescale Λ must be faster than the protein dynamics, so that protein expression does not fluctuate, and slower than the TF dynamics, so that the TF is near its steady state values for most of the light pulse duration. To quantify these conditions, a "tracking score" is defined for the TF dynamics, and an "integration score" for the protein dynamics, which require simulations of the full system. A quantitative explanation for the linearity of the PWM curves is not provided.

Ultimately, the model (61) finds good agreement with experimental data, and yet its analysis in Ref. [34] remains perplexing. It is not clear how to systematically extend the transient tracking and integration scores to more complex systems. The mRNA dynamics are largely ignored, no score is associated to the mRNA although in the discussion it is mentioned that they too limit the PWM period. Thus, the practitioner looking to build upon this system may be left thinking that these full system simulations are necessary to tune the pulse widths, and may be uncertain regarding the constraints imposed by the mRNA dynamics. Our aim is to demonstrate how a multiple-scales analysis dispenses with these ad-hoc scores, replacing them with explicit requirements for obtaining the desired PWM results.

4.2. Revisiting the PWM analysis

We begin the analysis by nondimensionalising the model via the scalings

$$\begin{aligned} T &= \frac{T_{\text{tot}}}{1+k_{\text{off}}/(v_{\max}k_{\text{on}})}\hat{T}, & R &= \frac{k_{\text{basal}}+k_{\max}}{k_{\text{degR}}}\hat{R}, \\ K &= \frac{T_{\text{tot}}}{1+k_{\text{off}}/(v_{\max}k_{\text{on}})}\hat{K}, & P &= \frac{k_{\text{trans}}}{k_{\text{degP}}}\frac{k_{\text{basal}}+k_{\max}}{k_{\text{degR}}}\hat{P}, \\ t &= \frac{\hat{t}}{k_{\text{degP}}}, \end{aligned} \tag{63}$$

where we have chosen to scale time on the protein degradation timescale. Along with the state variables, we also denote the light input on the dimensionless timescale: $v(t) = \hat{v}(\hat{t})$. The scalings (63) were chosen to reflect the characteristic concentrations of each species. To see this, note that, after dropping the hats to declutter the notation, system (61) takes the form

$$\frac{k_{\text{degP}}}{v(t)v_{\max}k_{\text{on}}+k_{\text{off}}}\frac{\mathrm{d}T}{\mathrm{d}t} = \frac{v(t)(v_{\max}k_{\text{on}}+k_{\text{off}})}{v(t)v_{\max}k_{\text{on}}+k_{\text{off}}} - T, \tag{64a}$$

$$\frac{k_{\text{degP}}}{k_{\text{degR}}}\frac{\mathrm{d}R}{\mathrm{d}t} = \left[1 - \frac{1}{1+(T/K)^n}\frac{1}{1+k_{\text{basal}}/k_{\max}}\right] - R, \tag{64b}$$

$$\frac{\mathrm{d}P}{\mathrm{d}t} = R - P. \tag{64c}$$

The form (64) allows a particularly simple explanation of the dynamics: each dependent variable tracks the first quantity on the right-hand side, on the timescale given by the coefficient of the time derivative on the left-hand side. Since the light input is bounded $0 \leq v(t) \leq 1$, it follows that the inhomogeneity in the T-dynamics is always on the interval $[0,1]$. Therefore, T remains $O(1)$, and thus so too do R and P, as well as their steady states. We deduce that the scalings (63) reflect the typical concentrations in the cell, regardless of how we choose the parameters. Moreover, this wealth of information was available without having to solve a single differential equation. Nonetheless, the transient dynamics are responsible for the profile of the dose–response curves, and so we must study the time-dependence.

Turning our attention to the timescales, we see that the time t is scaled with the protein degradation k_{degP}, while the R dynamics unfold on a timescale of $O(k_{\text{degP}}/k_{\text{degR}})$. The T dynamics have a time-dependent timescale, varying from the slower scale $O(k_{\text{degP}}/k_{\text{off}})$ when the light is off, to the faster scale $O(k_{\text{degP}}/[v_{\max}k_{\text{on}}+k_{\text{off}}])$ at full light intensity (see Fig. A1 in Appendix A). In this particular application these are the same magnitudes (see Table 1), however, this observation is important for the general setting. For our purposes, the T timescale is required to be faster than the oscillation timescale, therefore, we take the slower timescale to give a stricter bound. Finally, to bring the system into the multiple-scales form, we rewrite the light input $v(t)$ as $u(t/\varepsilon)$ for the (dimensionless) period

$$\varepsilon = k_{\text{degP}}\Lambda, \tag{65}$$

and the functional form

$$u(\tau) = \sum_{i=-\infty}^{\infty} \mathbb{1}_{[0,r]}(\tau - i) = \mathbb{1}_{[0,r]}(\tau - \lfloor\tau\rfloor), \tag{66}$$

where $\lfloor\tau\rfloor$ denotes the largest integer less than or equal to τ, thus $\tau-\lfloor\tau\rfloor$ denotes the fractional part of τ. We then rewrite system (64), along with initial conditions, as

$$\delta\frac{\mathrm{d}T}{\mathrm{d}t} = u(t/\varepsilon)(\alpha+1)-(u(t/\varepsilon)\alpha+1)T, \qquad T(0)=T^0, \tag{67a}$$

$$\beta\frac{\mathrm{d}R}{\mathrm{d}t} = \left[1-\frac{1}{1+\gamma}\frac{1}{1+(T/K)^n}\right]-R, \qquad R(0)=R^0, \tag{67b}$$

$$\frac{\mathrm{d}P}{\mathrm{d}t} = R-P, \qquad P(0)=P^0, \tag{67c}$$

for

$$\alpha=\frac{v_{\max}k_{\mathrm{on}}}{k_{\mathrm{off}}}, \qquad \beta=\frac{k_{\mathrm{degP}}}{k_{\mathrm{degR}}}, \qquad \gamma=\frac{k_{\mathrm{basal}}}{k_{\max}}, \qquad \delta=\frac{k_{\mathrm{degP}}}{k_{\mathrm{off}}}. \tag{68}$$

Our aim is to solve (67) in the asymptotic limit of fast oscillations: $\varepsilon\to 0$. The period used for experiments in Ref. [34] is $\varepsilon=0.21$ (see (65) and Table 1). The TF timescale $\delta\approx 0.02\ll\varepsilon$ and our intent is ultimately to consider TF dynamics faster than the v-oscillations. Nevertheless, we consider the richer asymptotic limit in which $\delta=O(\varepsilon)$, which will allow us to consider separate sources of error in isolation. This is an application of the Principle of Minimal Simplification in Refs. [3, 35], and highlights that there may in fact be several different timescales of relevance in the dynamics. The focus on the ε scale separation is a useful partition between "fast" and "slow" groups, but does not negate the possibility of scales within each group. Importantly, the case of $\delta\ll\varepsilon$ may be studied within the $\delta=O(\varepsilon)$ limit, since this richer limit preserves the $\delta\ll\varepsilon$ case as a (singular) limit.

With $\delta=O(\varepsilon)$, the transcription factor T is a fast species, while the protein P is a slow species, and we must decide how β scales in the limit as $\varepsilon\to 0$, that is, whether the mRNA, R, is a slow or a fast species. For the experimental parameters in Table 1 we see that $\beta\approx 0.17$ and is thus small. Nonetheless, we consider both the limit of fast mRNA ($\beta=O(\varepsilon)$) and slow mRNA ($\beta=O(1)$), and, in the first instance, we assume that $\beta=O(1)$. Analysing both cases sheds light on the nature of the multiple-scales approximation, and allows us to draw conclusions relevant for arbitrary values of β.

In seeking a multiple-scales solution to the nonlinear system (67), we could pose it in the general nonlinear form as described in Section 2.1. However, the exposition is more concise and lucid if the perturbative analysis is performed directly on the ODE system (67). Introducing the fast timescale $\tau=t/\varepsilon$ on which the solution is assumed periodic, and assuming τ to be independent of the slow timescale t, we apply the multiple-scales operator (3) to yield the governing system

$$\delta\frac{\partial T}{\partial t}+\frac{\delta}{\varepsilon}\frac{\partial T}{\partial\tau} = u(\tau)(\alpha+1)-(u(\tau)\alpha+1)T, \tag{69a}$$

$$\beta\frac{\partial R}{\partial t}+\frac{\beta}{\varepsilon}\frac{\partial R}{\partial\tau} = \left[1-\frac{1}{1+\gamma}\frac{1}{1+(T/K)^n}\right]-R, \tag{69b}$$

$$\frac{\partial P}{\partial t}+\frac{1}{\varepsilon}\frac{\partial P}{\partial\tau} = R-P, \tag{69c}$$

Expanding T, R, and P as an asymptotic series in powers of ε,

$$T\sim T_0+\varepsilon T_1+\cdots, \qquad R\sim R_0+\varepsilon R_1+\cdots, \qquad P\sim P_0+\varepsilon P_1+\cdots, \tag{70}$$

we find, upon substituting (70) into (69), that the leading-order solution satisfies

$$\frac{\delta}{\varepsilon}\frac{\partial T_0}{\partial \tau} = u(\tau)(\alpha+1) - (u(\tau)\alpha+1)T_0, \qquad \frac{\partial R_0}{\partial \tau} = 0, \qquad \frac{\partial P_0}{\partial \tau} = 0. \tag{71}$$

We are interested in the case of TF dynamics faster than the ε timescale, which motivates the limit $\delta/\varepsilon \ll 1$. Since u is piecewise constant, this singular limit introduces boundary layers of width $O(\delta/\varepsilon)$ in the vicinity of each switch in the light profile, beyond which the approximation is exponentially accurate. For a comprehensive discussion on this approximation, see Appendix A. We deduce that, in the fast-TF limit $\delta/\varepsilon \ll 1$, the TF is well approximated by $T_0 \sim u(\tau)(\alpha+1)/[u(\tau)\alpha+1]$, from which it follows that

$$T_0 \sim u, \tag{72}$$

since $u(t) \in \{0,1\}$ in our application (see (66)). For R_0 and P_0, we see from (71) that these vary only on the slow timescale, which is determined at the next order. Averaging the $O(1)$ terms in (69) over the fast period, we find that

$$\beta\frac{\mathrm{d}R_0}{\mathrm{d}t} = \eta_0 - R_0, \qquad \frac{\mathrm{d}P_0}{\mathrm{d}t} = R_0 - P_0, \tag{73}$$

where, with the help of (72), η_0 is given by

$$\eta_0 = 1 - \frac{1}{1+\gamma}\int_0^1 \frac{1}{1+(T_0/K)^n}\,\mathrm{d}\tau \sim \left(1 - \frac{1}{1+\gamma}\right) + r\left(\frac{1}{1+\gamma}\frac{1}{1+K^n}\right). \tag{74}$$

We solve (73) explicitly in Appendix B, however, it is more enlightening at this stage to focus on the large-time behaviour, which is given simply by P_0, $R_0 \sim \eta_0$. From Table 1, we see that $\gamma \ll 1$, and, therefore, in practice we expect the response P_0 to be effectively linear with respect to r. This is precisely what is observed experimentally in Ref. [34]. Using the multiple-scales framework we have complemented the experimental observation with a model-based quantification.

4.3. Clarifying the assumptions

It is instructive to reflect on what we have assumed and what this allowed us to calculate. We assumed the timescale hierarchy $\delta \ll \varepsilon \ll 1$, and that $\beta = O(1)$.

Requiring $\delta \ll \varepsilon$ guarantees that the TF dynamics will be faster than the input signal oscillations, thus ensuring the "tracking" score is high, while $\varepsilon \ll 1$ guarantees that the oscillations are faster than the protein dynamics, ensuring that the protein fluctuations are small and thereby the "integration" score is low. We thus see how the timescale hierarchy assumption replaces the need for any ad-hoc scores requiring full numerical simulations of the system and extensive transient information.

The timescale hierarchy translates into explicit dimensional inequalities:

$$\delta \ll \varepsilon \ll 1 \qquad \Longleftrightarrow \qquad \frac{1}{k_{\mathrm{off}}} \ll \text{Pulse width } (\Lambda) \ll \frac{1}{k_{\mathrm{degP}}}, \tag{75}$$

which are more straightforward for the practitioner to check than transient scores. For example, the results in Ref. [34] show that for a period of 7.5 min the PWM regime is weakened. This corresponds to $\varepsilon \approx 0.053$ where the assumption $\delta \ll \varepsilon$ is weaker.

The second assumption required $\beta = O(1)$. What happens if the mRNA timescale is asymptotically fast, whereby $\beta = O(\varepsilon)$? The leading-order mRNA dynamics (69b) become

$$\frac{\beta}{\varepsilon}\frac{\partial R_0}{\partial \tau} = \left[1 - \frac{1}{1+\gamma}\frac{1}{1+(T_0/K)^n}\right] - R_0, \tag{76}$$

varying periodically in τ on the fast timescale at leading order. Using τ-periodicity it follows from (76) that

$$\int_0^1 R_0 \,\mathrm{d}\tau = \eta_0. \tag{77}$$

The protein dynamics are still τ-independent and to be determined at first order, where we find, after averaging over the fast timescale in (69c) and using (77), that

$$\frac{\mathrm{d}P_0}{\mathrm{d}t} = \int_0^1 R_0 \,\mathrm{d}\tau - P_0 = \eta_0 - P_0. \tag{78}$$

whereby the same large-time protein behaviour is recovered: $P_0 \sim \eta_0$.

Ultimately, both regimes produce the same large-time behaviour at leading order, and agree excellently with full numerical simulations (see Fig. 5b). We find that small deviations from the affine profile occur at extreme duty cycles $r \approx 0$ and $r \approx 1$ (Fig. 5b inset). Since these are not predicted in the $\delta/\varepsilon \ll 1$ limit (see Fig. A2 in Appendix A), but are reproduced in the $\delta = O(\varepsilon)$ limit, we deduce that these are the result of finite-δ/ε effects: When duty cycle r is nearly zero or unity, the input signal is nearly constant, with deviations only for short time intervals. In this case, the boundary layers associated with the singular limit occupy these short time intervals, and are thus no longer negligible (see Appendix A for an extended discussion).

For large $\beta \gg 1$, the mRNA dynamics decelerate the protein variations to the mRNA timescale, allowing for an even longer pulse period. Assumption (75) may thus be relaxed, in the case of general β, to

$$\frac{1}{k_{\mathrm{off}}} \ll \text{Pulse width } (\Lambda) \ll \frac{1}{k_{\mathrm{degP}}} + \frac{1}{k_{\mathrm{degR}}}. \tag{79}$$

The general condition (79) provides a more complete (that is, including mRNA stability) and more straightforward (that is, in closed form, requiring no simulation) characterisation than previously reported of the assumptions required to achieve the PWM regime of interest.

The discussion in Section 3.2 demonstrates that higher-order perturbations not only capture the high-frequency oscillations but can reveal additional deviations from the time-averaged structure. This motivates a higher-order analysis of system (69).

4.4. Higher-order perturbations

In this section we pursue higher-order perturbations, in both the case of fast mRNA ($\beta = O(\varepsilon)$) and slow mRNA ($\beta = O(1)$). The results presented in this section use T_0 given by (A.2) for which $\delta = O(\varepsilon)$. As detailed in Appendix A, this form exhibits exponentially small errors. In this way, we isolate the sources of error: approximation errors in this section may be assumed to stem from the order of the multiple-scales solution or the scale of β chosen.

We seek higher-order solutions of (69) that capture the oscillations in both the mRNA and protein solutions. The calculations are a direct application of the theory derived in Section 2,

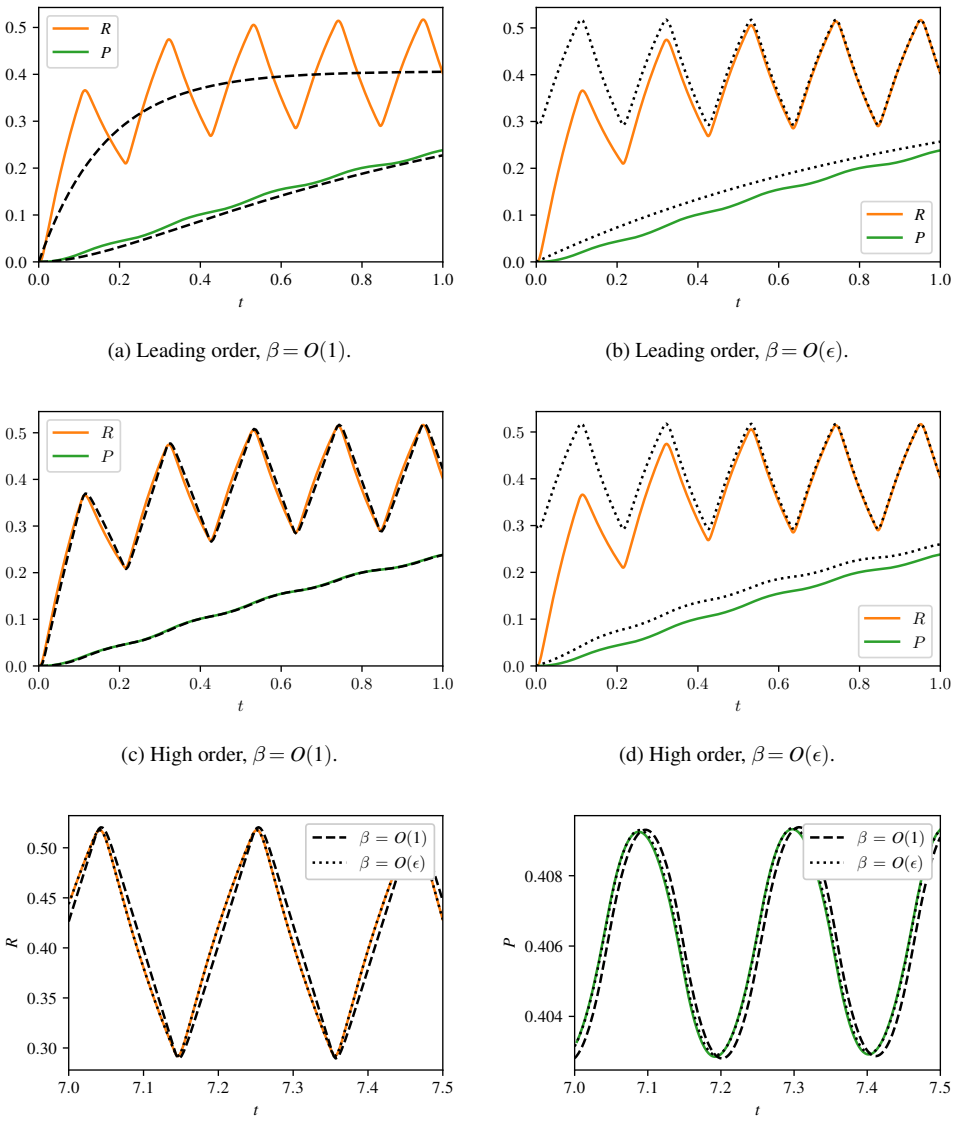

(a) Leading order, $\beta = O(1)$.

(b) Leading order, $\beta = O(\epsilon)$.

(c) High order, $\beta = O(1)$.

(d) High order, $\beta = O(\epsilon)$.

(e) Large time.

(f) Large time.

Figure 6. mRNA (R) and protein (P) dynamics. Solid curves show the full numerical solution of system (67) while broken curves show the asymptotic approximations derived in Appendix B. Parameters for the 5 BS system were used (see Table 1).

and are performed for both mRNA timescales in Appendix B. As previously observed, when assuming $\beta = O(1)$, the mRNA and protein solutions do not vary on the fast timescale. The oscillations are captured in the mRNA at first order R_1 and at second order in the protein P_2. This is because T is driven by the oscillations, while R is driven by T, and P is driven by R. Therefore, the oscillations, which are captured by the $(1/\varepsilon)\partial/\partial\tau$ derivative, propagate through at successively higher order. For this same reason, when $\beta = O(\varepsilon)$, the oscillations

are captured at leading order in the mRNA R_0 and at first order in the protein P_1. One striking outcome of this derivation is that the fluctuations in protein concentration are of order $O(\varepsilon^2)$ if $\beta = O(1)$, but of order $O(\varepsilon)$ if $\beta = O(\varepsilon)$. In the former case, we see from (B.8) and (B.17) that the high-frequency perturbations scale as $1/\beta$, and thus the more general scaling of $O(\varepsilon^2/\beta)$ includes the case of $\beta \gg 1$.

This observation is important for the practitioner. Since small protein fluctuations are desirable [34], even if a practical range of k_{degR} has little effect on the pulse-period condition (79), it may nevertheless have a significant impact on the protein fluctuations. This quantification thus provides the practitioner with the appropriate scaling law to aid experimental design.

To recap, we have computed both leading-order and higher-order approximations of system (67), in both the cases of $\beta = O(1)$ and $\beta = O(\varepsilon)$. Comparing these four solutions provides deeper insight into the multiple-scales asymptotics. In Figs. 6a–6d we depict the four solutions computed over the same time horizon.

When $\beta = O(1)$ the leading order (Fig. 6a) shows no oscillations in either the mRNA or protein, but the time-averaged profiles satisfy the initial conditions and closely match the trend of the dynamics. At higher order (Fig. 6c), the initial condition remains satisfied, and the oscillations are captured. The agreement is good, however, the fluctuations show small but persistent deviations.

When $\beta = O(\varepsilon)$, the leading order (Fig. 6b) captures the oscillations in the mRNA but not the protein. Since the multiple-scales ansatz is τ-periodic, the mRNA does not satisfy the initial conditions. This explains why the protein profile overestimates the true solution. At higher order (Fig. 6d) the oscillations in the protein are captured. While the oscillations match the true solution qualitatively, the mRNA periodicity still results in the multiple-scales solution to be an overestimate of the true protein concentration.

The plots in Fig. 6 illustrate the approximations obtained using different scaling assumptions about β, but the same numerical value of β (to match the parameters in Table 1). This might seem perplexing at first glance, since it seems that the $\beta = O(1)$ limit outperforms the $\beta = O(\varepsilon)$ limit, despite using the parameter value $\beta \approx 0.17 < 0.21 = \varepsilon$. It might be tempting to suggest that, just as the case of $\delta \ll \varepsilon$ may be studied in the $\delta = O(\varepsilon)$ limit, here too even though $\beta \ll 1$, the $\beta = O(1)$ limit encapsulates this case. However, in this case, our calculations have shown that the $\beta = O(\varepsilon)$ limit is not preserved by the $\beta = O(1)$ limit: the leading-order R dynamics differ between these cases because R is a fast species in the former limit but a slow species in the latter.

The reason the less suitable limit outperforms the more suitable limit initially is that the $\beta = O(1)$ limit encapsulates a leading-order contribution that is not τ-periodic and thus it can satisfy the initial conditions. This provides for good agreement early on, but is ultimately limited by the fact that the parameters do not strongly satisfy the asymptotic assumptions. On the other hand, the $\beta = O(\varepsilon)$ limit is in agreement with the parameter choice, but the multiple-scales periodicity negates the possibility of satisfying arbitrary initial conditions, and thus at early times the approximation suffers. In fact, this problem carries over to the TF dynamics as well, it just so happens that the periodic multiple-scales solution deviates from the initial condition by only an exponentially small amount (see Appendix A for a further discussion). At larger times (Figs. 6e and 6f) order is restored and the $\beta = O(\varepsilon)$ approximation is more accurate than the $\beta = O(1)$ approximation in capturing the limit-cycle behaviour.

That periodicity precludes an arbitrary initial condition from being satisfied is reminiscent of the quasi-steady state assumption (QSSA) not satisfying an arbitrary initial condition (as discussed in Section 1). Here too a boundary layer is present when the initial condition deviates substantially from the limit cycle, whereby the periodicity assumption

is initially inaccurate. Nonetheless, the fast species converge rapidly to their limit cycle behaviour whereupon the approximation accuracy is restored. Should one wish, just as with a singular perturbation, a boundary layer analysis can be performed in the vicinity of the initial time, where the full dynamics of the fast species are recovered, and thus arbitrary initial conditions may be satisfied.

Our multiple-scales analysis uncovers explicit scaling laws for system concentrations, and reveals concrete system requirements to achieve the PWM regime. We are able to more comprehensively and explicitly quantify and thus explain experimental results, while exhibiting remarkable agreement with the full nonlinear numerical simulations with a significantly simplified approximation obtainable in closed form.

5. Conclusions

In this paper, we apply the method of multiple scales to fast–slow systems with a rapidly oscillating periodic parameter or input signal. We develop the general nonlinear theory, obtaining formally closed systems governing the perturbations at every order. In the particularly important case of biaffine systems — which include components bilinear in the system state and oscillations, linear in the state only, linear in the oscillations, as well as inhomogeneous — we obtain closed systems governing all orders. Notably, this class of systems includes those arising from the chemical master equation and its continuum approximations.

We demonstrate the application of the biaffine theory when the oscillations are faster than the underlying system dynamics. In this case, we find that the leading-order asymptotic approximation coincides with the intuition that the system responds to the averaged input signal. Several key features of the method arise from the examples presented. Notably, in many real-world processes unfolding at disparate timescales, the timescale separation is moderately large, but not infinite, in which case the system response deviates significantly from the its response to the time-averaged signal. We demonstrate how the method extends beyond the elementary intuition of a time-averaged signal (relevant only in the absence of fast species), by resolving higher-order perturbations that capture the oscillatory system response. We find that the higher-order system response does not, in general, have zero mean on the fast timescale. This further highlights the importance of the higher-order terms, revealing how the solution deviates from the leading order, not only by oscillations but also by slow-timescale corrections.

The examples demonstrate how the multiple-scales approach achieves significant complexity reduction by structurally embedding the timescale separation into the approximation form. This approach disentangles the disparate timescales, allowing the dynamics on each to be resolved independently.

We revisit a system of nonlinear equations describing a fast–slow system previously studied in the literature. We show how our multiple-scales framework sheds light on the underlying assumptions of the system, replacing full numerical simulations and ad-hoc metrics by explicit, static expressions. We show how different numerical simulations may also be explained by explicit analytical expressions previously unreported. Formal scaling laws, including estimates of the oscillation magnitude, reveal a crisper quantitative picture regarding how the desired experimental regime may be achieved. Here too, the structure underpinning these results is the timescale separation that is leveraged by the multiple-scales analysis.

Finally, we discuss how the fast-time periodicity, which is needed to close the multiple-scales equations at each order, excludes the possibility of imposing an arbitrary initial

condition for the fast species. This can lead to a boundary layer in the vicinity of the initial time, when the full solution is not near enough its limit cycle to be near periodic. This is akin to the QSSA which fails to satisfy arbitrary initial conditions. Just as with the QSSA, a boundary layer analysis restores the full fast dynamics near the initial time and captures the evolution from arbitrary initial conditions towards the limit-cycle behaviour.

Several previous studies have dealt with system reduction and approximation techniques for biological applications (for example, Ref. [36] provides a comprehensive survey in stochastic biochemical kinetics). The most prominent approach in the context of fast–slow systems is the quasi-steady state approach, where fast dynamics are reduced to their quasi-steady state reducing the system exclusively to the slow dynamics. In the Introduction we demonstrate why this approach does not yield insight beyond the intuitive idea of replacing the rapidly oscillating signal by its time average. This shortcoming sets this work apart from classical fast–slow systems. The multiple-scales approach developed allows for coarse-grained evolution while retaining the influence of the fast oscillations.

Some previous work exploiting timescale separation is applicable to oscillatory systems [37]. Other approximation approaches have been studied on oscillatory systems without recourse to timescale separation [38]. The key difference between the current work and these studies is that we assume the presence of an externally applied, rapidly oscillating signal. While the method of multiple scales is an applicable tool for rapid, endogenous oscillations (that is, those arising from the system dynamics rather than externally applied), the analysis performed here would need to be suitably adapted. In contrast, the timescale separation is crucial: the oscillations must be fast with respect to the slow dynamics, which is not the case in these two studies: Ref. [38] does not rely on well separated timescales, and even though Ref. [37] mentions oscillations, these arise from the reduction of a system with fast species, in other words, the oscillations occur on the slow timescale after the fast dynamics have been reduced, and are thus of a different nature to those studied here. On the other hand, we pursued a perturbative analysis that extends to arbitrary order, and provides formal error estimates. Much of the previous work cited falls short of these two features. Timescale separation is assumed in Ref. [37], nevertheless, higher-order approximations are not pursued. Ref. [38], while also assuming a fairly specific biochemical reaction network structure, develops an ad-hoc approximation without anaytical control over the error.

In various application there may exist more than two timescales of interest [39], and multiple spatial scales of interest. The methodology expounded in this work may be directly extended to tackle these cases.

Appendix A. Dynamics of the transcription factor

The T dynamics in (67a) decouple from the rest of the system, and we rewrite the leading-order contribution governed by (71):

$$\frac{\delta}{\varepsilon}\frac{\partial T_0}{\partial \tau} = u(\tau)(\alpha+1) - (u(\tau)\alpha+1)T_0. \tag{A.1}$$

Recall from (66) that $u(\tau) = \mathbb{1}_{[0,r]}(\tau - \lfloor \tau \rfloor)$ for $\tau \in [0,1]$. Therefore, when the light is on, the solution is given by

$$T_0 = 1 + c(t)\mathrm{e}^{-(\alpha+1)\varepsilon\tau/\delta}, \tag{A.2a}$$

while in the dark, the solution is given by

$$T_0 = d(t)\mathrm{e}^{-\varepsilon\tau/\delta}. \tag{A.2b}$$

The values $c(t)$ and $d(t)$ are constants of integration with respect to τ. They are determined by imposing continuity of T_0 as the light is switched off at $\tau = r$, as well as τ-periodicity, to give

$$c = \frac{\mathrm{e}^{-(1-r)\varepsilon/\delta} - 1}{1 - \mathrm{e}^{-(1+\alpha r)\varepsilon/\delta}}, \qquad d = \frac{\mathrm{e}^{r\varepsilon/\delta} - \mathrm{e}^{-\alpha r\varepsilon/\delta}}{1 - \mathrm{e}^{-(1+\alpha r)\varepsilon/\delta}}. \tag{A.2c}$$

These values are constants with respect to t, thus $\partial T_0/\partial t = 0$, and at the next order,

$$\frac{\delta}{\varepsilon}\frac{\partial T_0}{\partial t} + \frac{\delta}{\varepsilon}\frac{\partial T_1}{\partial \tau} = -(u(\tau)\alpha + 1)T_1. \tag{A.3}$$

Since T_0 does not vary with t, the only τ-periodic solution of (A.3) is zero. This is true for all orders, and reflects the fact that the multiple-scales approximation (A.1) retains all terms of the original (67a).

In the fast-TF limit $\delta/\varepsilon \ll 1$, the leading-order T_0 is given by solving (A.1) when neglecting the time derivative on the left-hand side, namely

$$T_0 \sim \frac{u(\tau)(\alpha+1)}{u(\tau)\alpha + 1}, \qquad \text{therefore} \qquad T_0 \sim u(\tau) \qquad \text{when} \qquad u \in \{0,1\}, \tag{A.4}$$

as in our case (see (66)). For piecewise constant u, the form of the leading order T_0 in (A.4) is also piecewise constant, and therefore its τ-derivative is zero almost everywhere. It follows from (A.1) that this outer approximation is accurate to all orders, that is, if we expand T_0 asymptotically with respect to δ/ε, all asymptotic corrections are zero. This observation coincides with the solution (A.2): when $\delta/\varepsilon \ll 1$, we see that, when τ is not within a vicinity of width $O(\delta/\varepsilon)$ of switches in the light profile $\tau \in \{0, r\}$, the two solutions coincide up to exponentially small corrections.

The condition of τ not being in the vicinity of light switches is a consequence of the fast-TF case being a singular limit: for piecewise constant u, neglecting the τ-derivative introduces boundary layers of width $O(\delta/\varepsilon)$ beyond each point in time the light signal switches. A matched asymptotic expansion resolves the dynamics within the boundary layers. Denote $\tau = \tau_0$ a switch in the light profile, where $u(\tau_0^-) := \lim_{\tau\uparrow\tau_0} u(\tau) = 1 - \lim_{\tau\downarrow\tau_0} u(\tau) =: 1 - u(\tau_0^+)$, and scaling τ locally near τ_0 via

$$\tau = \tau_0 + \frac{\delta}{\varepsilon}\xi, \tag{A.5}$$

equation (A.1) takes the form

$$\frac{\partial T_0}{\partial \xi} = \begin{cases} (\alpha+1)(1-T_0), & u(\tau_0^+) = 1, \\ -T_0, & u(\tau_0^+) = 0, \end{cases} \tag{A.6a}$$

along with the initial condition given by the outer solution on the time interval up to $\tau = \tau_0$, namely

$$T_0(0) = u(\tau_0^-). \tag{A.6b}$$

Problem (A.6) admits the solution

$$T_0 = \begin{cases} 1 - \mathrm{e}^{-(\alpha+1)\xi}, & u(\tau_0^+) = 1, \\ \mathrm{e}^{-\xi}, & u(\tau_0^+) = 0, \end{cases} \tag{A.7}$$

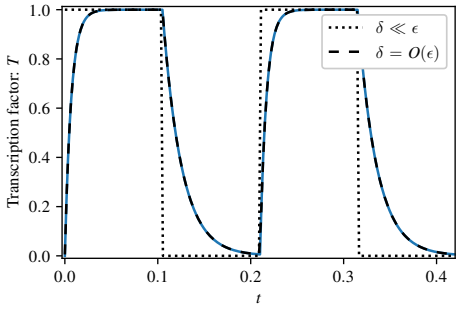

Figure A1. TF dynamics. The solid curve is the exact solution of (67a), while the broken curves depict asymptotic approximations. The dashed curve illustrates the multiple-scales solution (A.2) retaining the τ-dependence by considering $\delta = O(\varepsilon)$, while the dotted curve illustrates the quasi-steady form (A.4) obtained by assuming that $\delta \ll \varepsilon$.

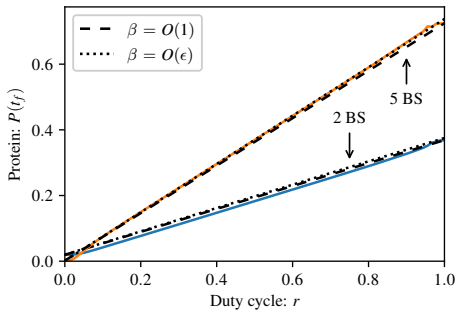

Figure A2. Dose–response curves in the PWM regime for different genetic constructs (see Table 1) for a terminal time of $t_f = 360 k_{\text{degP}}$, which corresponds to 6 hours. Solid curves show full numerical solutions of system (67), while broken curves show the leading-order multiple-scale approximation given by (B.3) and (B.26) and using piecewise constant T_0 in (A.4). The asymptotic approximations are only slightly worse than for the exponentially-accurate T_0 used in Fig. 5b.

which we see matches the outer solution: $T_0 \to u(\tau_0^+)$ as $\xi \to \infty$. The solution (A.7) may be written on the original timescale for $\tau \in [0,1]$ by undoing (A.5), which gives

$$T_0 = \begin{cases} 1 - \mathrm{e}^{-(\alpha+1)\varepsilon\tau/\delta}, & \tau < r, \\ \mathrm{e}^{-(\tau-r)\varepsilon/\delta}, & \tau > r. \end{cases} \tag{A.8}$$

The multiple-scales solution (A.2) is continuous and periodic, but exhibits an exponentially small deviation from the zero initial condition in (67a). The matched asymptotic solution (A.8) satisfies the zero initial condition, but exhibits an exponentially small discontinuity at switching points. While the simple form (A.4) does exhibit noticeable discrepancy from the other solutions (Fig. A1), it remains a useful limiting form to obtain analytical insight (as in Section 4.2) and exhibits very good agreement with the full numerical solution (see Fig. A2). This agreement will diminish when the duty cycle is sufficiently close to zero or unity, whereby the boundary layers are the dominant deviations from the constant light input profile and thus not negligible.

Since δ/ε is sufficiently small in our case, the exponentially small deviations are unnoticeable, and the multiple-scales, matched asymptotic, and exact solutions are indistinguishable (Fig. A1, the matched asymptotic solution is not shown but appears identical).

Finally, we note that the convergence of T to u is faster when turning the light on, than when turning the light off (Fig. A1). This reflects the observation made in Section 4.2 that the T timescale is time-varying.

Appendix B. Proceeding to higher order in the nonlinear system

In this appendix, we calculate the higher-order perturbations of R and P that capture the high-frequency oscillations, in both the case of slow ($\beta = O(1)$) and fast ($\beta = O(\varepsilon)$) mRNA dynamics.

Appendix B.1. Slow mRNA dynamics

At leading order, we know from (71) that R_0 and P_0 do not depend on τ. At first order,

$$\beta\frac{\mathrm{d}R_0}{\mathrm{d}t}+\beta\frac{\partial R_1}{\partial\tau}=1-h(\tau)-R_0, \tag{B.1a}$$

$$\frac{\mathrm{d}P_0}{\mathrm{d}t}+\frac{\partial P_1}{\partial\tau}=R_0-P_0, \tag{B.1b}$$

where

$$h(\tau)=\frac{1}{1+\gamma}\frac{1}{1+(T_0(\tau)/K)^n}. \tag{B.2}$$

Integrating (B.1) over one τ-period produces (73), which is solved by

$$R_0=\eta_0+(R_0^0-\eta_0)\mathrm{e}^{-t/\beta}, \tag{B.3a}$$

$$P_0=P_0^0\mathrm{e}^{-t}+\eta_0(1-\mathrm{e}^{-t})+\frac{R_0^0-\eta_0}{1-1/\beta}(\mathrm{e}^{-t/\beta}-\mathrm{e}^{-t}), \tag{B.3b}$$

with η_0 defined in (74).

We now seek the fast-timescale perturbations in R and P. To this end, we derive the higher-order dynamics from (69), whereby, for $i\geq 0$,

$$\beta\frac{\partial R_{i+1}}{\partial\tau}=\mathbb{1}_{i=0}(1-h(\tau))-R_i-\beta\frac{\partial R_i}{\partial t}, \tag{B.4a}$$

$$\frac{\partial P_{i+1}}{\partial\tau}=R_i-P_i-\frac{\partial P_i}{\partial t}. \tag{B.4b}$$

The first term on the right-hand side of (B.4a) includes the factor $\mathbb{1}_{i=0}$ which takes the value one for $i=0$ and takes the value zero for all other i. Averaging over one τ-period and imposing periodicity with respect to τ, we see that, for $i\geq 1$,

$$\beta\frac{\mathrm{d}}{\mathrm{d}t}\int_0^1 R_i\,\mathrm{d}\tau=-\int_0^1 R_i\,\mathrm{d}\tau, \tag{B.5a}$$

$$\frac{\mathrm{d}}{\mathrm{d}t}\int_0^1 P_i\,\mathrm{d}\tau=\int_0^1 R_i\,\mathrm{d}\tau-\int_0^1 P_i\,\mathrm{d}\tau. \tag{B.5b}$$

Given R_j and P_j, equation (B.4) with $i = j$ may be integrated with respect to τ to give R_{j+1} and P_{j+1} up to unknown additive functions of t only. These unknown functions are determined by (B.5) with $i = j+1$, which guarantees τ-periodicity. With T_0, R_0, and P_0 in hand, our strategy is to determine perturbations of successively higher order.

We begin by calculating R_1. From (B.4a) with $i = 0$, and using (73) and (74), we obtain the fast-timescale R_1 variations

$$\beta \frac{\partial R_1}{\partial \tau} = 1 - h(\tau) - \eta_0 = \int_0^1 h(s)\,\mathrm{d}s - h(\tau). \tag{B.6}$$

Integrating (B.6) with respect to τ, we obtain

$$R_1 = c(t) + \tau H(1) - H(\tau), \tag{B.7}$$

where $c(t)$ is a constant of integration with respect to τ and

$$H(\tau) = \frac{1}{\beta}\int_0^\tau h(s)\,\mathrm{d}s. \tag{B.8}$$

Substituting (B.7) into (B.5b) with $i = 1$, it follows that

$$\beta \frac{\mathrm{d}c}{\mathrm{d}t} = -c - d, \tag{B.9}$$

for

$$d = \frac{H(1)}{2} - \int_0^1 H(\tau)\,\mathrm{d}\tau. \tag{B.10}$$

Equation (B.9) admits the solution

$$c(t) = \left(d + R_1^0\right)\mathrm{e}^{-t/\beta} - d, \tag{B.11}$$

for the initial condition R_1^0, and we have completely determined R_1.

We proceed to solve for P_1. We recall from (71) that R_0 and P_0 have no τ-dependence, and thus from (B.4b) and (B.5b) with $i = 0$, we find that

$$\frac{\partial P_1}{\partial \tau} = 0. \tag{B.12}$$

Therefore, P_1 does not vary with τ, but may vary on the slow timescale. From (B.7), (B.10) and (B.11), we calculate

$$\int_0^1 R_1\,\mathrm{d}\tau = c(t) + d = \left(d + R_1^0\right)\mathrm{e}^{-t/\beta}. \tag{B.13}$$

Substituting (B.13) into (B.5b) with $i = 1$, we obtain

$$\frac{\mathrm{d}P_1}{\mathrm{d}t} = \int_0^1 R_1\,\mathrm{d}\tau - P_1 = \left(d + R_1^0\right)\mathrm{e}^{-t/\beta} - P_1, \tag{B.14}$$

which is solved by

$$P_1 = \begin{cases} \dfrac{d + R_1^0}{1 - 1/\beta}\left(\mathrm{e}^{-t/\beta} - \mathrm{e}^{-t}\right) + P_1^0\mathrm{e}^{-t}, & \beta \neq 1, \\ \left(d + R_1^0\right) t\,\mathrm{e}^{-t} + P_1^0\,\mathrm{e}^{-t}, & \beta = 1 \end{cases} \tag{B.15}$$

To obtain the oscillations in P we must proceed to higher order. From (B.4b) with $i = 1$ and (B.7), (B.11) and (B.13) we see that

$$\frac{\partial P_2}{\partial \tau} = R_1 - \int_0^1 R_1 \,\mathrm{d}\tau = \tau H(1) - H(\tau) - d, \tag{B.16}$$

from which it follows, after integration with respect to τ, that

$$P_2 = q(t) - \tau d + \frac{\tau^2 H(1)}{2} - \int_0^\tau H(s)\,\mathrm{d}s, \tag{B.17}$$

for an unknown $q(t)$. Substituting (B.17) into (B.5b) with $i = 1$, we see that

$$\frac{\mathrm{d}}{\mathrm{d}t}\int_0^1 P_2 \,\mathrm{d}\tau = \int_0^1 R_2 \,\mathrm{d}\tau - \int_0^1 P_2 \,\mathrm{d}\tau. \tag{B.18}$$

To obtain the τ-integral term on the right-hand side of (B.18), we must proceed to higher order for R. Continuing just as before (without detailing the intermediate steps), we find that

$$\int_0^1 R_2 \,\mathrm{d}\tau = \left(D + R_2^0\right)\mathrm{e}^{-t/\beta}, \tag{B.19}$$

for

$$D = \frac{d}{2} - \frac{H(1)}{6} + \int_0^1 \int_0^\tau H(s)\,\mathrm{d}s\,\mathrm{d}\tau. \tag{B.20}$$

Finally, substituting (B.17) and (B.19) into (B.18) and using (B.9), we derive an equation for q, namely

$$\frac{\mathrm{d}q}{\mathrm{d}t} = -q(t) + \left(D + R_2^0\right)\mathrm{e}^{-t/\beta} + D, \tag{B.21}$$

which is solved by

$$q(t) = \begin{cases} D + \dfrac{D + R_2^0}{1 - 1/\beta}\left(\mathrm{e}^{-t/\beta} - \mathrm{e}^{-t}\right) + \left(P_2^0 - D\right)\mathrm{e}^{-t}, & \beta \neq 1, \\ D + \left(D + R_2^0\right) t\,\mathrm{e}^{-t} + \left(P_2^0 - D\right)\mathrm{e}^{-t}, & \beta = 1. \end{cases} \tag{B.22}$$

This completely determines P_2, which capture the oscillations in the protein dynamics.

Appendix B.2. Fast mRNA dynamics

In this section we seek the perturbations that oscillate on the fast timescale in the $\beta = O(\varepsilon)$ case. The strategy is similar to the previous case of $\beta = O(1)$, however, the solution structure is importantly different.

For the R dynamics, we know that the leading-order contribution satisfies (76), where the oscillations are captured in R_0. The solution of (76) is given by

$$R_0 = c(t)\,\mathrm{e}^{-\tau\varepsilon/\beta} + H(\tau), \tag{B.23}$$

for an unknown $c(t)$, and where

$$H(\tau) = \frac{\varepsilon}{\beta}\int_0^\tau [1 - h(s)]\,\mathrm{e}^{(\varepsilon/\beta)(s-\tau)}\,\mathrm{d}s, \tag{B.24}$$

for h defined in (B.2). Imposing τ-periodicity, we find that

$$c = \frac{H(1)}{1 - \mathrm{e}^{-\varepsilon/\beta}}, \tag{B.25}$$

which does not depend on t. Just as with the T, all terms are retained in (76), and therefore all higher-order corrections in R are zero.

At leading order, the P dynamics satisfy (78), which is solved by

$$P_0 = \eta_0 + \left(P_0^0 - \eta_0\right)\mathrm{e}^{-t}, \tag{B.26}$$

for η_0 defined in (74). Oscillations in P are captured in P_1. From (B.4b) with $i = 0$ and (77) and (78), we find that P_1 is governed by

$$\frac{\partial P_1}{\partial \tau} = R_0 - \int_0^1 R_0 \,\mathrm{d}\tau = c\,\mathrm{e}^{-\tau\varepsilon/\beta} - \eta_0 + H(\tau). \tag{B.27}$$

Integrating (B.27) with respect to τ, we obtain

$$P_1 = C(t) - c\frac{\beta}{\varepsilon}\left(\mathrm{e}^{-\tau\varepsilon/\beta} - 1\right) - \tau\eta_0 + \int_0^\tau H(s)\,\mathrm{d}s, \tag{B.28}$$

for an unknown C. Substituting (B.28) into (B.4b) with $i = 1$ and recalling that $R_1 \equiv 0$, we derive the equation governing C, namely

$$\frac{\mathrm{d}C}{\mathrm{d}t} = -C(t) - D, \tag{B.29}$$

where

$$D = c\frac{\beta}{\varepsilon}\left[\frac{\beta}{\varepsilon}\left(\mathrm{e}^{-\varepsilon/\beta} - 1\right) + 1\right] - \frac{\eta_0}{2} + \int_0^1 \int_0^\tau H(s)\,\mathrm{d}s\,\mathrm{d}\tau. \tag{B.30}$$

Equation (B.29) is solved by

$$C(t) = \left(P_2^0 + D\right)\mathrm{e}^{-t} - D, \tag{B.31}$$

and thus we have determined P_1.

References

[1] G. Michel and G. P. Chini. Multiple scales analysis of slow–fast quasi-linear systems. *Proceedings of the Royal Society A*, 475(2223):20180630, 2019.

[2] J. Gunawardena. Time-scale separation–Michaelis and Menten's old idea, still bearing fruit. *The FEBS Journal*, 281(2):473–488, 2014.

[3] L. A. Segel and M. Slemrod. The quasi-steady-state assumption: A case study in perturbation. *SIAM Review*, 31(3):446–477, 1989.

[4] L. Michaelis and M. L. Menten. Die Kinetik der Invertinwirkung. *Biochemische Zeitschrift*, 49(37):333–369, 1913.

[5] J. K. Kim, K. Josić, and M. R. Bennett. The validity of quasi-steady-state approximations in discrete stochastic simulations. *Biophysical Journal*, 107(3):783–793, 2014.

[6] D. Barik, M. R. Paul, W. T. Baumann, Y. Cao, and J. J. Tyson. Stochastic simulation of enzyme-catalyzed reactions with disparate timescales. *Biophysical Journal*, 95(8):3563–3574, 2008.

[7] C. V. Rao and A. P. Arkin. Stochastic chemical kinetics and the quasi-steady-state assumption: Application to the Gillespie algorithm. *The Journal of Chemical Physics*, 118(11):4999–5010, 2003.

[8] R. Bundschuh, F. Hayot, and C. Jayaprakash. Fluctuations and slow variables in genetic networks. *Biophysical Journal*, 84(3):1606–1615, 2003.

[9] J. K. Kim and E. D. Sontag. Reduction of multiscale stochastic biochemical reaction networks using exact moment derivation. *PLOS Computational Biology*, 13(6):1–24, 06 2017.

[10] C. H. Lee and H. G. Othmer. A multi-time-scale analysis of chemical reaction networks: I. deterministic systems. *Journal of Mathematical Biology*, 60(3):387, 2010.

[11] B. Mélykúti, J. P. Hespanha, and M. Khammash. Equilibrium distributions of simple biochemical reaction systems for time-scale separation in stochastic reaction networks. *Journal of The Royal Society Interface*, 11(97):20140054, 2014.

[12] C. A. Gómez-Uribe, G. C. Verghese, and A. R. Tzafriri. Enhanced identification and exploitation of time scales for model reduction in stochastic chemical kinetics. *The Journal of Chemical Physics*, 129(24):244112, 2008.

[13] T. B. Kepler and T. C. Elston. Stochasticity in transcriptional regulation: Origins, consequences, and mathematical representations. *Biophysical Journal*, 81(6):3116–3136, 2001.

[14] P. Thomas, A. V. Straube, and R. Grima. The slow-scale linear noise approximation: an accurate, reduced stochastic description of biochemical networks under timescale separation conditions. *BMC systems biology*, 6(1):39, 2012.

[15] J. K. Kim, K. Josić, and M. R. Bennett. The relationship between stochastic and deterministic quasi-steady state approximations. *BMC systems biology*, 9(1):87, 2015.

[16] E. J. Hinch. *Perturbation Methods*. Cambridge Texts in Applied Mathematics. Cambridge University Press, 1991.

[17] N. Fenichel. Geometric singular perturbation theory for ordinary differential equations. *Journal of Differential Equations*, 31(1):53–98, 1979.

[18] M. Desroches, J. Guckenheimer, B. Krauskopf, C. Kuehn, H. M. Osinga, and M. Wechselberger. Mixed-mode oscillations with multiple time scales. *SIAM Review*, 54(2):211–288, 2012.

[19] J. R. Bowen, A. Acrivos, and A. K. Oppenheim. Singular perturbation refinement to quasi-steady state approximation in chemical kinetics. *Chemical Engineering Science*, 18(3):177–188, 1963.

[20] L. Ashall, C. A. Horton, D. E. Nelson, P. Paszek, C. V. Harper, K. Sillitoe, S. Ryan, D. G. Spiller, J. F. Unitt, D. S. Broomhead, D. B. Kell, D. A. Rand, V. Sée, and M. R. H. White. Pulsatile stimulation determines timing and specificity of nf-κb-dependent transcription. *Science*, 324(5924):242–246, 2009.

[21] C. K. Dalal, L. Cai, Y. Lin, K. Rahbar, and M. B. Elowitz. Pulsatile dynamics in the yeast proteome. *Current Biology*, 24(18):2189–2194, 2014.

[22] M. H. Holmes. *Introduction to perturbation methods*, volume 20. Springer Science & Business Media, 2012.

[23] J. K. Kevorkian and J. D. Cole. *Multiple scale and singular perturbation methods*, volume 114. Springer Science & Business Media, 2012.

[24] N. N. Bogoliubov and Y. A. Mitropolsky. *Asymptotic methods in the theory of non-linear oscillations*. Hindustan Publishing Corporation, 1961.

[25] I. V. Andrianov and L. I. Manevitch. *Asymptotology: ideas, methods, and applications*, volume 551. Springer Science & Business Media, 2002.

[26] M. R. Bennett, D. Volfson, L. Tsimring, and J. Hasty. Transient dynamics of genetic regulatory networks. *Biophysical Journal*, 92(10):3501–3512, 2007.

[27] N. G. van Kampen. *Stochastic processes in physics and chemistry*. North Holland, third edition, 2007.

[28] C. Gardiner. *Stochastic Methods: A Handbook for the Natural and Social Sciences*. Springer Series in Synergetics. Springer Berlin Heidelberg, third edition, 2009.

[29] H. Risken. *Fokker–Planck Equation*. Springer Berlin Heidelberg, Berlin, Heidelberg, 1996.

[30] R. Grima, P. Thomas, and A. V. Straube. How accurate are the nonlinear chemical fokker-planck and chemical langevin equations? *The Journal of Chemical Physics*, 135(8):084103, 2011.

[31] W. Weidlich and G. Haag. *Concepts and models of a quantitative sociology: the dynamics of interacting populations*, volume 14. Springer Science & Business Media, 2012.

[32] D. Lunz. On continuum approximations of discrete-state markov processes of large system size. *Multiscale Modeling and Simulation*, 2021. Accepted.

[33] D. Lunz, G. Batt, J. Ruess, and J.-F. Bonnans. Beyond the chemical master equation: stochastic chemical kinetics coupled with auxiliary processes. https://hal.inria.fr/hal-02991103.

[34] D. Benzinger and M. Khammash. Pulsatile inputs achieve tunable attenuation of gene expression variability and graded multi-gene regulation. *Nature Communications*, 9(1):1–10, 2018.

[35] M. Kruskal. Asymptotology. In S. Drobot and P. A. Viebrock, editors, *Mathematical Models in Physical Sciences*, pages 17–48. Prentice-Hall, Englewood Cliffs, N.J., 1963. Proceedings of the Conference at the University of Notre Dame.

[36] D. Schnoerr, G. Sanguinetti, and R. Grima. Approximation and inference methods for stochastic biochemical kinetics — a tutorial review. *Journal of Physics A: Mathematical and Theoretical*, 50(9):093001, 2017.

[37] P. Thomas, R. Grima, and A. V. Straube. Rigorous elimination of fast stochastic variables from the linear noise approximation using projection operators. *Phys. Rev. E*, 86:041110, Oct 2012.

[38] Z. Cao and R. Grima. Linear mapping approximation of gene regulatory networks with stochastic dynamics.

Nature communications, 9(1):1–15, 2018.

[39] J. Gunawardena. A linear framework for time-scale separation in nonlinear biochemical systems. *PLOS ONE*, 7(5):1–14, 05 2012.